TECHNISCHE
UNIVERSITÄT
WIEN
Vienna University of Technology

ESEA
Institut für Energiesysteme
und Elektrische Antriebe

Modelling and Combined Simulation of a Power-to-Gas Process

MASTER THESIS

In partial fulfillment of the requirements for the degree

Diplom-Ingenieur (Dipl.-Ing.)

committed by

Univ.-Prof. Dr. techn. Wolfgang Gawlik
Dipl. Ing. Sabina Begluk

of the

Vienna University of Technology

Faculty of Electrical Engineering and Information Technology
Institute of Energy Systems and Electrical Drives

By
Andreas Fleischhacker
Kleine Neugasse 9/17
1050 Vienna
Austria

10.09.2013, Vienna

"Das Wasser ist die Kohle der Zukunft. Die Energie von morgen ist Wasser, das durch elektrischen Strom zerlegt worden ist. Die so zerlegten Elemente des Wassers, Wasserstoff und Sauerstoff, werden auf unabsehbare Zeit hinaus die Energieversorgung der Erde sichern."

Jules Verne, Die geheimnisvolle Insel, 1870

Abstract

The expansion of renewable energy sources increases constantly in today's energy supply. Renewable energy sources are characterised by high volatility, which requires an increasing number of energy storage systems. Pump storage and storage power plants store electrical energy and enable to postpone its consumption. Another way of storing electrical energy offers the Power-to-Gas concept. Power-to-Gas converts electrical energy into hydrogen or methane and enables the storage in the gas grid.

This work contains a high-detailed mathematical model of a Power-to-Gas plant in MATLAB®/SIMULINK. Further a simulation of the model in two different medium voltage grids over the period of one year is carried out. The Power-to-Gas plant's model is split up in two units. The first unit comprises the model of an alkaline electrolyser. The second unit depicts the model of methanation. Conclusions about the Power-to-Gas plant's dynamic and overall efficiency are obtained by the mathematical model. Additionally critical parameters and the limits of a Power-to-Gas plant are identified.

An inclusion of the Power-to-Gas plant in two distribution grids examines if an operation with a high share of renewable energy sources is possible and sensible. Combined simulation leads to different plant sizes differentiating in capacity, energy input, overall efficiency and in the quantity of full-load hours per year. At the end strategies concerning the operation of a Power-to-Gas plant are discussed.

Kurzzusammenfassung

In der heutigen elektrischen Energieversorgung werden regenerative Energiequellen stetig ausgebaut. Diese weisen eine sehr hohe Volatilität auf, wodurch der Bedarf an elektrischen Energiespeichern ansteigt. Eine Möglichkeit der Speicherung von elektrischer Energie, neben den bestehenden Pumpspeicher- und Speicherkraftwerken, bietet das Power-to-Gas Konzept. Hiermit ist es möglich elektrische Energie, durch Umwandlung in Wasserstoff oder Methan, in dem Gasnetz zu speichern.

Diese Arbeit behandelt zunächst eine exakte mathematische Modellierung einer Power-to-Gas Anlage in MATLAB®/SIMULINK, welche danach in typischen Mittelspannungsnetzen über den Zeitraum eines Jahres simuliert wird. Das Modell der Power-to-Gas Anlage kann in zwei Abschnitte unterteilt werden. Den ersten Abschnitt, welcher einen Großteil des Modells der Power-to-Gas Anlage ausmacht, umfasst das Modell eines alkalischen Elektrolyseurs. Der zweite Abschnitt beschreibt das Modell einer Methanisierung. Das mathematische Modell ermöglicht Aussagen über die Dynamik und den Gesamtwirkungsgrad einer Power-to-Gas Anlage zu tätigen. Weiters identifiziert es kritische Parameter und zeigt die Grenzen einer solchen Anlage auf.

Die Einbindung des Power-to-Gas Modells in zwei Mittelspannungsnetze untersucht, ob der Betrieb mit einem hohen Anteil an regenerativen Energiequellen möglich und sinnvoll ist. Diese kombinierte Simulation führt zu unterschiedlichen Anlagengrößen, welche sich bezüglich der Auslastung, des Energieinhalts, des Wirkungsgrads und der Volllaststundenzahl unterscheiden. Am Ende der Arbeit werden Strategien für den Betrieb einer Power-to-Gas Anlage angeführt.

Contents

List of Figures

List of Tables

Acronyms

CH_4 . . . . methane

CO_2 . . . . carbon dioxide

H_2 . . . . hydrogen

AEL . . . . Alkaline Electrolysers

CCGT . . . . Combined Cycle Gas Turbine

GT . . . . Gas Turbine

P2G . . . . Power-to-Gas

PEM . . . . Proton Exchange Membrane

PEMEL . . . . Proton Exchange Membrane Electrolysers

PV . . . . photovoltaic

RPM . . . . Renewable Power Methane

SBCR . . . . Slurry Bubble Column Reactor

SNG . . . . Synthetic Natural Gas

SOEL . . . . Solid Oxid Electrolysers

WP . . . . wind power

1. Introduction

Typical electrical energy sources are powerful power plants, providing centrally energy-supply for consumers. In Austria a huge amount of these power plants is fossil fired and delivers the electrical energy by a hierarchic grid structure to the consumer. Today an increasing number of consumers produce energy by photovoltaic. Additionally installed windpower raises. A part of this renewable energy is often fed back into the grid.

A disadvantage of renewable energy producers is their dependency on nature's behaviour. Therefore renewable energy plants are characterised with much lower full load hours than conventional power plants. As a consequence the residual load power is fluctuating in the positive and negative direction. This problem can be solved with the use of electrical storage systems. Not only short-time but also seasonal storage systems will be required for a sustainable energy supply. According to the study Super-4-Micro-Grid [48] it is not possible to guarantee a 100% renewable energy supply in Austria with only pump storage and storage power plants. Even an extensive expansion of pump storage power plants will not be enough to solve the storage problem.

Another possibility of storing electrical energy is to transform it and store it in the gas grid. An advantage of this method is the higher flexibility of the gas grid in comparison to the electrical grid. The injected gas (energy carrier in the gas grid) has not to be consumed at the moment of injection, while the electrical energy (energy carrier in the electrical grid) has to be consumed at the point in time of generating it. Another reason depicts the much higher storage capacity of the gas grid, because Austria's gas grid provides several pore storages [14]. Energy density of chemical storage systems is much higher, than the energy density of hydraulic power plants. The conversation process of electrical energy into a gas substitute is known in literature as P2G Process [46].

The P2G Process consists of two processes, the electrolysis and the methanation. Electrolysis produces hydrogen using electrical energy to split water. The produced hydrogen can directly be used or can in combination with carbon dioxide be transformed into synthetic methane. Similar characteristics of Synthetic Natural Gas (SNG) to natural gas enable the feeding-in of synthetic methane into the gas grid. Besides SNG it is possible to feed-in small quantities of hydrogen in the gas grid as well [40].

The main target of the Master thesis *"Modelling and combined Simulation of a Power-to-Gas Process"* is the determination of a mathematical model and it's implementation in the numerical software tool MATLAB®/SIMULINK. This high-detailed model enables the investigation of a P2G plant's dynamic and its limiting parameters. Another part of this

work is the implementation of the P2G plant model in two representative middle-voltage grids, a typical rural and a typical suburban grid. These two grids include renewable energy sources. The rural grid consists of PV power plants at the consumers' roofs and a WP park, while the suburban grid only includes the consumers' PV plants without any other renewable energy sources. The operation of the P2G model over a year with the grid's negative residual load power shows the annual energy consumption of the P2G plant at different plant sizes. The P2G plant in these grids operates in two modes, which results in different efficiencies. Another subject of the investigation is the operation of a P2G plant in two modes. Generated SNG via the P2G plant depends on injected electrical energy. The result of efficiency, i.e. the relation of SNG to injected energy, is shown over the period of a year. The achievable full load hours of the P2G plant depending on the grid and the operation mode are a further subject.

This work is divided into the following chapters.

- *Chapter 2 "Motivation"*, describes the main idea behind this work.

- *Chapter 3 "Mathematical Modelling of the P2G Process"*, explains the electrolyser's and methanation's mathematical background.

- *Chapter 4 "Representative Electrical Grid Models"*, gives an overview of two grid topologies and their characteristics such as load, photovoltaic and wind power profiles.

- *Chapter 5 "Combined Simulation"*, contains the combined simulation's analysis of the P2G model of Chapter 3 in the grids introduced in Chapter 4.

- *Chapter 6 "Summary and Outlook"*, implies a final review of this work's results.

- *Chapter A "Numerical Values"*, includes all numerical values of the parameters appearing in this thesis.

2. Motivation

The structure of today's energy supply is starting to change. The growing part of regenerative energy production causes the economic inviability of fossil fueled power plants. According to the master plan 2020 the regenerative energy generation has to increase [52]. As mentioned in the introduction chapter, the renewable energy sources are characterised by a significant disadvantage, volatility of energy production. For example the main amount of PV energy is produced midday. Seasonal dependence of the renewable energy generation exists too, e.g. PV power production is maximum during summer months and WP production during the translational period and winter months.

Today back-up power plants must be ready for operation to generate balancing energy, ensuring energy supply for customers. The need for balancing energy increases with a growing share of renewable energy production [13],[12]. This kind of energy compensation is not optimised due to efficiency and emissions. On the other hand regenerative energy sources often produce energy in the period of low demand. In order to reduce the energy surplus, renewable power plants are shut down. This occurrence can be avoided with the use of electrical energy storage systems [39]. Electrical energy storage enables a shift in time from high power to low power periods.

Austria's common used electrical storage systems are pump storage and storage power plants. Austria has already installed large pump storage capacity, but the required expansion of this storage capacities is hardly possible. The study's "Super-4-Micro-Grid" [48] conclusion is that even with a large-scale expansion of pump storage and storage power plants, it is not possible to ensure a 100% regenerative energy supply in Austria. For that reason it is necessary to use new storage technologies simultaneously with the expansion of regenerative energy sources. The following chapter gives an overview of the common used storage technologies and presents especially the P2G concept.

2.1. Storage Technologies

The principals of the most energy storage systems are based on the knowledge of the last two centuries, but research made some significant progresses in last years. It is possible to store electrical energy without transformation in systems like coils and capacitors. Most of storage systems transform electrical energy into another form of energy to store it. The reconversion is done by converting it back into electrical energy. This process is connected with transformation losses, an important parameter for storage systems. Essential arguments of these storage systems are the robustness and cycle stability of the
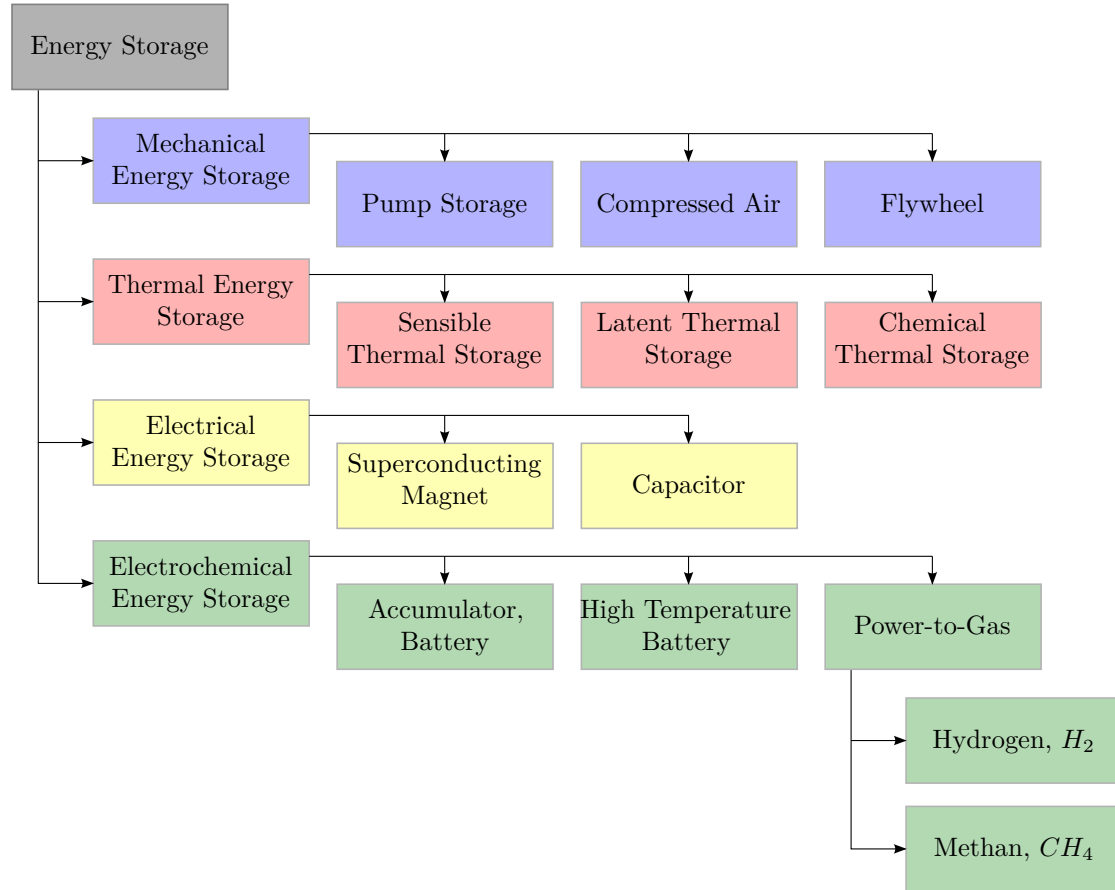
Figure 2.1.: An overview of electrical energy storage systems, without any claim to completeness. Picture based on [39].

system [39].

According to Figure 2.1 the most important storage systems can be split up in four categories. They can be differentiated in four energy forms mechanical, thermal, electrical and electrochemical. Each category shows some typical storage systems. The P2G technology belongs to electrochemical storage systems and is the essential storage system of this work. Further details of the shown storage systems are available in [39].

2.2. The Power-to-Gas Concept

Today typically pumped storage and pressed air plants are used to store larger amounts of electrical energy. Both storage technologies are limited due to [31],[48]. The P2G concept is an innovative way to store electrical energy, by linking the electrical and the
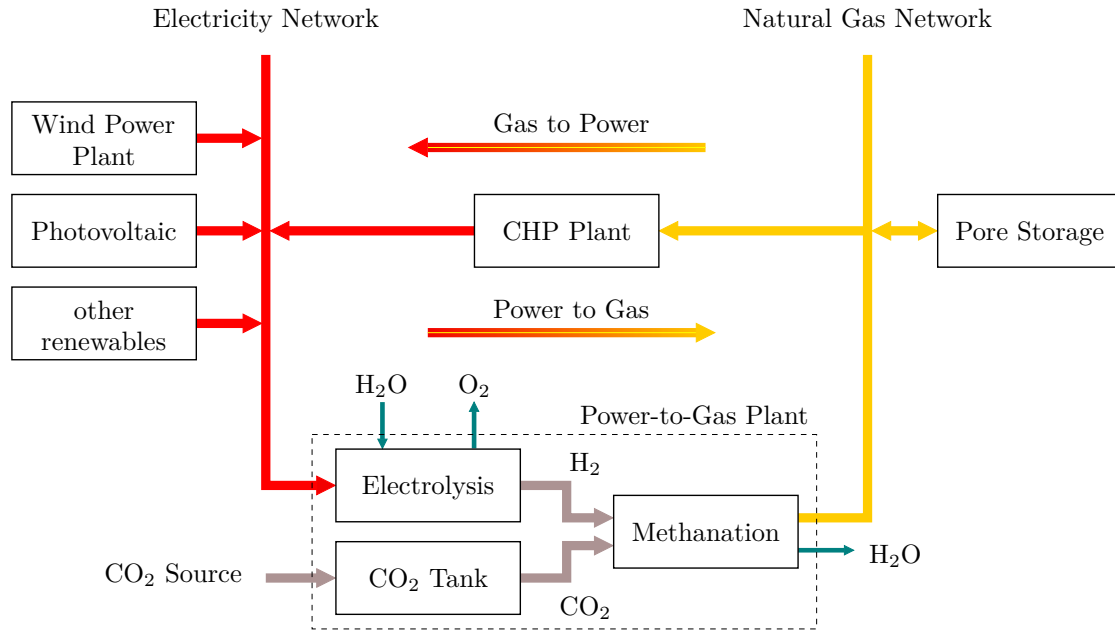
Figure 2.2.: The concept to store the renewable power in the natural gas grid by transforming electrical power into methane. Picture based on [46]

gas grid in both directions. Surplus energy can be shifted temporarily with the use of the gas grid.

As it is illustrated in Figure 2.2, the P2G plant connects the electricity network to the natural gas network. Electrolysis generates hydrogen by using electricity to split up water. This step transforms the electrical into chemical energy. Austria has no hydrogen structure, but the 4mol% can be fed into the natural gas grid [40]. A further step in the P2G process is the methanation to combine hydrogen with CO_2 and generate methane. If the electrical power for this process is generated by renewable power generation, the methane is called Renewable Power Methane (RPM) or SNG [46].

Methane's advantages over hydrogen are

- storages of methane - the natural gas grid - is available,

- higher energy density of methane to hydrogen and

- the transfer capacities of gas pipelines are much higher than these of electrical grids.

The synthetic methane or hydrogen can be stored or re-converted to electricity with gas turbines and/or combined cycle power plants and fuel cells. A by-product of the methanation process is heat that can be used for district heat, local heat or industrial
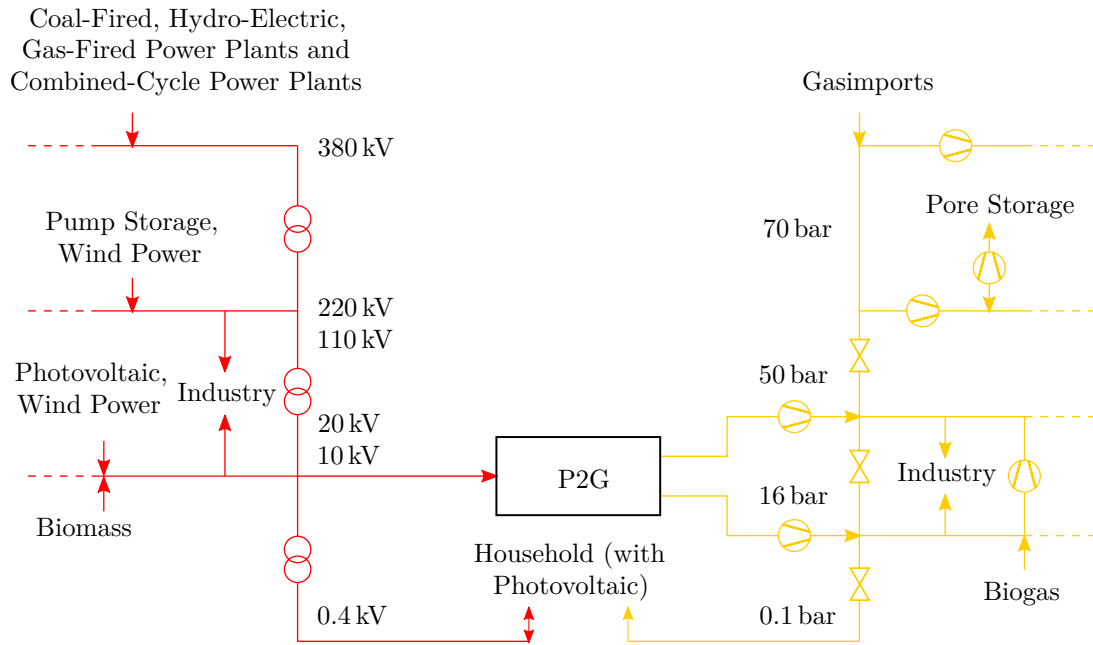
Figure 2.3.: Gas and electrical grid with typical levels and exemplary producers and consumers. Picture based on [5]

processes. Besides the technical advantages P2G enables Austria to reduce it's energy dependency on countries like Russia. Germany already operates P2G pilot projects [2],[17].

2.3. Implementation in Austria

The gas grid besides the electrical grid is the second largest power grid and the largest power storage of Austria [15],[18],[16]. By comparing the power consumption of electricity in the year 2011 of 60.4 TWh to the capacity of Austria's usable gas storage capacity of 75 TWh[1] it is obvious that no other storage system is providing such a high storage capability [12],[14]. Another possibility is to use the storage capabilities of the gas grid itself, as an advantage to the electrical grid, the volume putted in has not to be consumed at the same time.

According to [8] Austria's natural gas grid is differentiated in transmission and distribution levels. Gas transported in the transmission system does not directly supply the consumers itself. The consumer's gas supply is provided by systems in the distribution level which can be split up in

---

[1]calculated with the lower heating value of natural gas of [44]

- distribution systems of grid level 1,

- distribution systems of grid level 2 with a system pressure > 6 bar and

- distribution systems of grid level 3 with a system pressure ≤ 6 bar.

The feed-in of synthetic methane in Austria's grid was one of the Bachelor thesis's [16] topics. The work investigated advantages and disadvanteges of SNG input in different natural gas levels. The gas grid is highly seasoned due to the temperature depending customers. To guarantee a constant high input volume over the whole year the injection of SNG in natural gas grid levels 1 and 2 is advisable. In these levels the pressure goes up to 70 bar, but higher compressor losses have to be considered [16]. If the volume input is made in level 3 with a system pressure ≤ 6 bar the Austrian-wide energy potential is only about 2.5 TWh/a [23].

Figure 2.3 shows the link of electrical grid and natural gas grid. It also illustrates today's energy supply built up by central and decentral power plants and consumers like industry and households. The pressure levels of natural gas grid are presented exemplary, because pressure levels of the gas grid vary a lot. While the electrical grid levels are separated by transformers, the gas grid levels are parted by pressure valves. The valves control the required pressure of the lower grid levels. Compressors in transmission level guarantee a constant gas pressure over the grid level or increase the pore storage's input gas pressure. The P2G and Biogas plants' compressors increase the SNG's pressure to enable the fed-in in the gas grid.

This work is examining the connection of a P2G plant and the electrical distribution grid. Due to today's available literature the dynamic behaviour of a P2G plant is unknown. For that reason the first part of the work is the development and verification of a P2G plant's accurate mathematical model. As shown in this chapter the P2G plant consists of an electrolyser and a methanation. The essential component for the P2G plant's dynamic is the electrolyser. As mentioned at the beginning, renewable energy sources are characterised by a high volatility in energy production. The electrolyser's dynamic has to be sufficient following high energy gradients of the renewable energy sources, to store the maximum of renewable energy. A high-detailed electrolyser model indicates critical parameters e.g. the required standby power and the internal electrolyser temperature[2].

By including the model of the P2G plant in the two distribution grids of [38], it is possible to simulate the "real time" behaviour of a P2G model over the period of a year. A subject of investigation is if the operation with a high share regenerative produced energy is possible. In order to guarantee a (N-1) criterion of the grid, the position of the P2G in the grids is investigated. The optimal position of the P2G plant increases the potential of renewable energy sources expansion in the grid. As shown in [38] different P2G plant sizes cause a changed energy content of the P2G plant. An advanced optimisation of

---

[2]Other objects of the electrolysers inquiry are the efficiency, temperature dependency, and cooling demand of the electrolyser.

the P2G plant size, due to maximum efficiency and energy content is another subject of this work. A reduction of the P2G plant size increases the efficiency of the plant and results in higher full load hours. The combined simulation of the P2G plant model and the electrical grid also leads to different operation modes of the P2G plant. The operation modes are differentiated by the required standby power[3]. This work examines the operation mode with a standby power of 15% and the minimum operation load with 30% of the P2G plant's nominal power. An important difference of the P2G plant's operation modes is that the hydrogen (H_2) purity at the standby mode is to poor for further use[4]. Another difference of two operation modes is the grid's external power consumption, which is much higher at the minimum operation mode. The different operation modes result in miscellaneous full load hours and efficiencies of the plant.

---

[3]Alkaline electrolyser are not able to work beyond the standby power.

[4]The P2G plant's power have to stay at least at the standby power to manage an increasing power input.

3. Mathematical Model of the Power-to-Gas Process

This chapter describes the mathematical model of a typical P2G Process. The model consists of two parts as shown in Figure 3.1. The first element depicts the electrolyser, the gateway to the electrical grid. H_2 produced by the electrolyser reacts with carbon dioxide (CO_2) in the catalyser and produces SNG, water and heat. The heat generation and usage is not investigated in this work.

The model's input

$$\mathbf{x}_{in,P2G}(t) = [P_{P2G}(t), N_P, N_S]^T \tag{3.1}$$

consists of the electrical power $P_{P2G}(t)$ and the amount of parallel stacks N_P and serial cell elements N_S. The model's output

$$\mathbf{y}_{out,P2G}(t) = \left[\dot{V}_{H_2,AEL}(t), \dot{V}_{CH_4,meth}(t), \dot{V}_{H_2O,AEL}(t), \dot{V}_{H_2O,meth}(t), \dot{V}_{CO_2,meth}(t)\right]^T \tag{3.2}$$
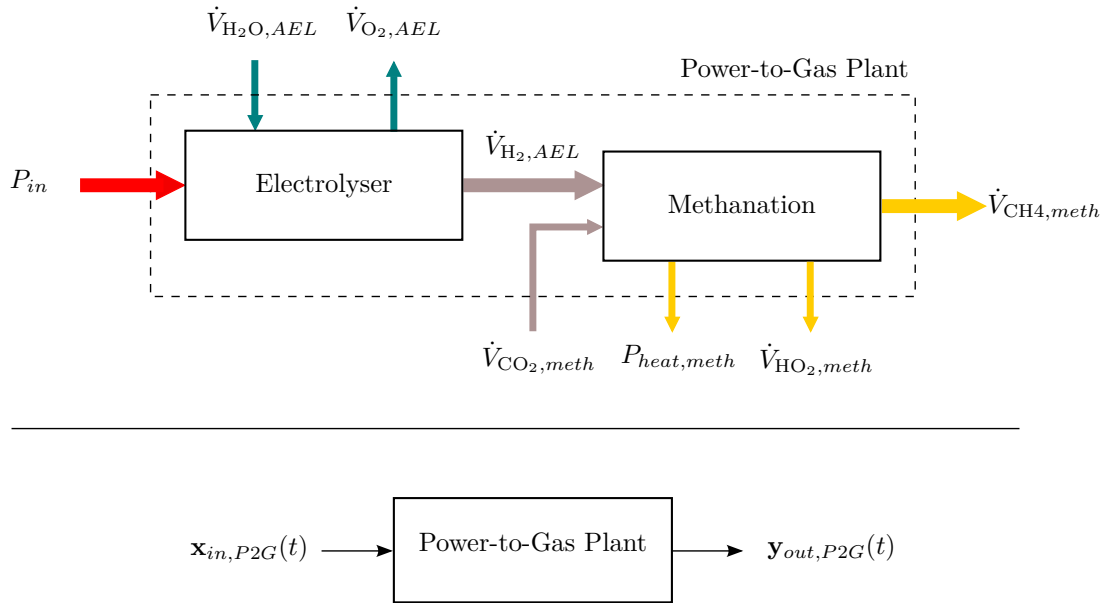
Figure 3.1.: Structure, in- and outputs of the P2G Model
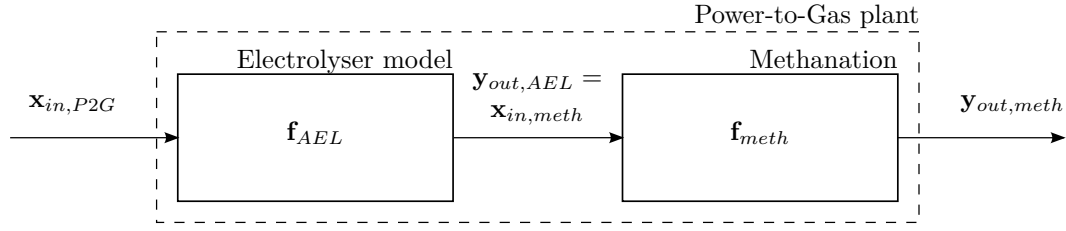
Figure 3.2.: Structure of the P2G Model consisting of an electrolyser and a methanation

consists of the flow rate of hydrogen $\dot{V}_{H_2,AEL}(t)$ and the flow rate of water needed for the electrolysis $\dot{V}_{H_2O,AEL}(t)$. These output variables are produced by the electrolyser. Another part of the output is generated by methanation, the flow rate of methan $\dot{V}_{CH_4,meth}(t)$, water $\dot{V}_{H_2O,meth}(t)$ and CO_2 for the methanation $\dot{V}_{CO_2,meth}(t)$. A more detailed explanation of the electrolyser and methanation pictured in Figure 3.2 follows in Sections 3.1 and 3.2.

 To relieve the readability, time dependence of the variables is assumed, but not written e.g.

$$\mathbf{x}_{in,P2G}(t) \mathrel{\widehat{=}} \mathbf{x}_{in,P2G}. \tag{3.3}$$

3.1. Electrolyser

The electrolyser, the P2G model's first part converts electrical energy into a chemical energy carrier, hydrogen. The beginning of this Section describes the process in the electrolyser and different types of electrolysers. The second part of this section presents a detailed model of an electrolysis process consisting of an electrochemical and a thermal model.

3.1.1. Types of electrolysers

According to [41] and [44] the three main types of electrolysers are

- the *Alkaline Electrolysers (AEL)*,

- the *Proton Exchange Membrane Electrolysers (PEMEL)* and

- the *high temperature (HTEL)* e.g. *Solid Oxid Electrolysers (SOEL)*,

which are listed up in Table 3.1, containing further characteristics. The information of the following paragraphs is based on [41] and [44].

Alkaline electrolysers use a porous diaphragm of ceramics (e.g. NiO) or synthetics (e.g. polysulphone) to separate the H_2 and O_2 flow. The diaphragm is gas-proof, has a low electrical resistance and a high mechanical stability. The liquid electrolyte is based on an about 30% wt. KOH solution. Today alkaline electrolysers are commercial available as

Technology	Electrolyte	Change carrier	Reactant	Temperature	Operating Range
AEL	Sodium or Patassium Hydroxide	OH^-	Water	$40 - 90\,°C$	$15 - 100\%$
PEMEL	Polymer	H^+	Water	$20 - 100\,°C$	$0 - 100\%$
HTEL (SOEL)	Ceramic	O^{2-}	Water, CO_2	$700 - 1000\,°C$	$0 - 100\%$

Table 3.1.: Types of electrolysers and characteristic parameters [44],[26]

large scale units ($> 1\,\text{MW}$) and are long term tested [41].

Proton Exchange Membrane (PEM) electrolysers include a proton exchange conductive polymer electrolyte, that separates the oxygen producing anode to the hydrogen producing cathode. PEMEL are preferred in low power applications, because of the raising life expectancy and their better dynamic range to AEL's [44]. Disadvantageous of AEL in contrast to PEMEL is their usage of a KOH solution, because KOH is a corrosive liquid.

High temperature electrolysis enabels the breakdown of water in steam at a ceramic anode (e.g. Ni/ZrO_2) and cathode (e.g. $LaMnO_3$). High temperature supports the endothermic reaction and reducing the demand of electricity about 25% [41]. The combination of high temperature electrolysers with processes like thermal power plants or solar heat promises huge potential in increase of total efficiency, by using their heat or steam. The disadvantages of HTEL are a long start-up time and material stress caused by mechanical and chemical processes [44].

The electrolyser modelled in this work is an AEL, because AEL reached a sufficient technology maturity and it is a State-of-the-Art technology in the hydrogen producing industry. It will take several years until PEM electrolysers are available as large scaled plant sizes like the AELs. The theory of this model can be used for an PEM electrolyser as well.

3.1.2. Model of an alkaline electrolyser

According to [10] the electrolysis reaction is

$$2\,H_2O(l) \longrightarrow 2H_2(g) + O_2(g), \; U_{rev,0} = 1.229\,V \qquad (3.4)$$
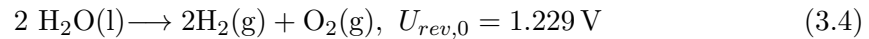
to decompose water. $U_{rev,0}$ is the required reversible voltage. The material's aggregate state liquid or gaseous is labelled by (l) or (g). As shown in Figure 3.3 the external current source cause two pair of electrons to flow from the anode to the cathode. According to
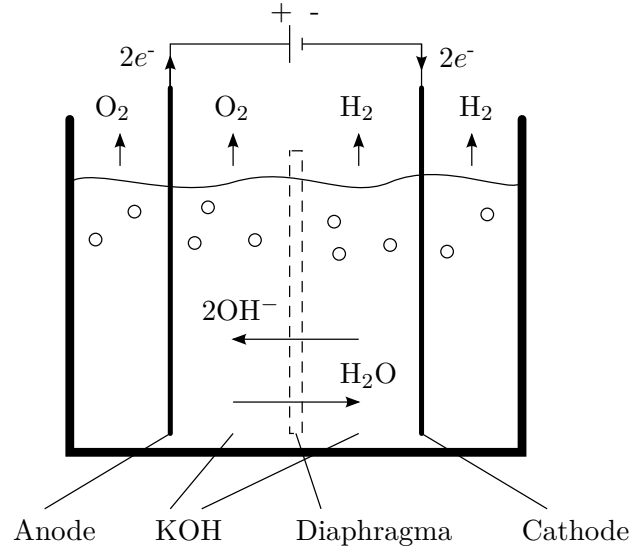
Figure 3.3.: Principle of an alkaline water electrolysis cell. Picture based on [41]

.

[51] the reaction (3.4) in an alkaline electrolyser can be split into an anodic

$$2\text{OH}^-(\text{l}) \longrightarrow \frac{1}{2}\text{O}_2(\text{g}) + \text{H}_2\text{O}(\text{l}) + 2e^- \tag{3.5}$$
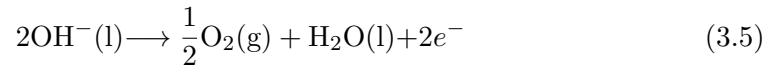
and into a cathodic reaction

$$2\text{H}_2\text{O}(\text{l}) + 2e^- \longrightarrow \text{H}_2(\text{g}) + 2\text{OH}^-(\text{l}). \tag{3.6}$$

At the cathodic side a pair of electrons cause the water split into hydrogen and hydroxide. The hydroxide molecule is shifted towards the anode side. At the anode oxygen, water and two electrons are released. To ensure a high conductivity of the electrolyte, alkaline electrolysers use a $20 - 40\%$ wt. KOH solution [44]. Therefore the electrodes have to be resistant to corrosion and have a low electrical resistance [49]. Table 3.2 shows the anodic and cathodic reaction of the three types of electrolysis of Section 3.1.1.

The basic equations of the following paragraphs are based on [41]. In combination with the assumptions of [49]

- hydrogen and oxygen are ideal gases,

- water is an incompressible fluid and

- the gases and liquid phases are separate,

following calculations can be facilitated. With these assumptions the Gibbs free energy

$$\Delta G = \Delta H + T \ \Delta S \tag{3.7}$$

Table 3.2.: Chemical anodic and cathodic reaction of the three types of electrolysers
according to [44],[26]

Technology	Anodic reaction	Cathodic reaction
AEL	$2OH^-(l) \rightarrow$ $\frac{1}{2}O_2(g) + H_2O(l) + 2e^-$	$2H_2O(l) + 2e^- \rightarrow$ $H_2(g) + 2OH^-(l)$
PEMEL	$2H^+(l) + 2e^- \rightarrow H_2(g)$	$H_2O(l) \rightarrow$ $\frac{1}{2}O_2(g) + 2H^+(l) + 2e^-$
HTEL	$H_2O(g) + 2e- \rightarrow$ $H_2(g) + O^{2-}(g)$	$O^{2-}(g) \rightarrow \frac{1}{2}O_2(g) + 2e^-$

of a general chemical reaction

$$v_{R,1} \; A_{R,1} + \cdots + v_{R,N_R} \; A_{R,N_R} \longrightarrow v_{P,1} \; B_{P,1} + \cdots + v_{P,N_P} \; B_{P,N_P} \tag{3.8}$$
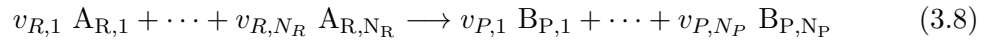
is defined as the sum of the enthalpy ΔH and the product temperature T with the entropy ΔS. The stoichiometric coefficients of the reactants $v_{R,1}, \ldots v_{R,N_R}$ and of the products $v_{P,1}, \ldots v_{P,N_P}$, define the amount of a substance quantity, necessary for reaction. $A_{R,1}, \ldots A_{R,N_R}$ and $A_{P,1}, \ldots A_{P,N_P}$ indicate the substance of chemical reaction. For example the reaction parameters of (3.4) are

$$v_{R,1} = 2, A_{R,1} = H_2O, N_R = 1, \tag{3.9}$$

$$v_{P,1} = 2, v_{P,} = 1, B_{P,1} = H_2, B_{P,2} = O_2 \text{ and } N_P = 2. \tag{3.10}$$

At standard ambient conditions ($p_{std} = 1$ bar and $T_{std} = 298.25$ K) the Gibbs-Helmholz equation (3.7)

$$\Delta G^\theta = \Delta H^\theta + T \; \Delta S^\theta \tag{3.11}$$

is written with the Index θ. The standard reaction enthalpy

$$\Delta H^\theta = \sum_{i=1}^{N_P} v_{P,i} \; \Delta H^\theta_{std,i} - \sum_{j=1}^{N_R} v_{R,j} \; \Delta H^\theta_{std,j} \tag{3.12}$$

consists of the standard formation enthalpies ΔH^θ_{std} of the elements in the general chemical equation (3.8). The same also applies for standard reaction entropy

$$\Delta S^\theta = \sum_{i=1}^{N_P} v_{P,i} \; S^\theta_{std,i} - \sum_{j=1}^{N_R} v_{R,j} \; S^\theta_{std,j}. \tag{3.13}$$

Therefore equation (3.11) is written by

$$\Delta G^\theta = \Delta H^\theta + T \; \Delta S^\theta$$
$$= \sum_{i=1}^{N_P} v_{P,i} \; \Delta H^\theta_{std,i} - \sum_{j=1}^{N_R} v_{R,j} \; \Delta H^\theta_{std,j} + T \left(\sum_{i=1}^{N_P} v_{P,i} \; S^\theta_{std,i} - \sum_{j=1}^{N_R} v_{R,j} \; S^\theta_{std,j} \right).$$
$$\tag{3.14}$$

At standard ambient conditions the thermodynamic parameters of the water electrolysis reaction (3.4) are

$$\Delta G^{\theta} = 237.21 \, \text{kJ/mol}, \ \Delta H^{\theta} = 285.84 \, \text{kJ/mol} \ \text{and} \ \Delta S^{\theta} = 178.03 \, \text{J/molK}. \qquad (3.15)$$

Faraday's law

$$Q = n \, z \, F \qquad (3.16)$$

describes the relation of the amount of a substance n, the charge number z, the Faraday constant $F = 96\,485 \, \text{As/mol}$ to the electrical charge Q. With electrical energy

$$E_{electr} = \Delta G = -Q \, U_{rev} \qquad (3.17)$$

and Faraday's law (3.16) for one mol ($n = 1 \, \text{mol}$) the conversion result is the reversible cell voltage

$$U_{rev} = -\frac{\Delta G}{z \, F} \, . \qquad (3.18)$$

The total energy demand necessary for electrolysis is the sum of enthalpy change ΔH and thermal irreversibility $T\Delta S$. The term $T\Delta S$ is the heat demand of the electrochemical process. Therefore the thermoneutral voltage

$$U_{th} = \frac{\Delta H}{z \, F} \qquad (3.19)$$

describes with the relation $1/zF$ the total energy demand, needed for the electrolysis. U_{th} is larger than the reversible voltage. At standard ambient conditions these voltages are

$$U_{rev,0} = 1.229 \, \text{V and} \ U_{th,0} = 1.482 \, \text{V} \, . \qquad (3.20)$$

Figure 3.4 shows the structure of the AEL model implemented in this work. The input matrix

$$\mathbf{T}_{in,AEL} = \begin{bmatrix} \eta_{AC/DC} & 0 & 0 \\ 0 & 1 & 0 \\ 0 & 0 & 1 \end{bmatrix} \qquad (3.21)$$

multiplies P_{P2G} of the input vector $\mathbf{x}_{in,P2G}$ with efficiency of the AC/DC rectifier. According to [42] efficiency $\eta_{AC/DC} = 99\%$. The model can be split into two submodels, into an electrochemical model with the output

$$\begin{aligned} \mathbf{y}_{out,AEL,ec} &= \mathbf{f}_{AEL,ec}(\mathbf{x}_{in,AEL}, \mathbf{y}_{out,AEL,th}) \\ &= \left[U_{AEL}, I_{AEL}, \dot{V}_{\text{H}_2}, \eta_e \right]^T \end{aligned} \qquad (3.22)$$
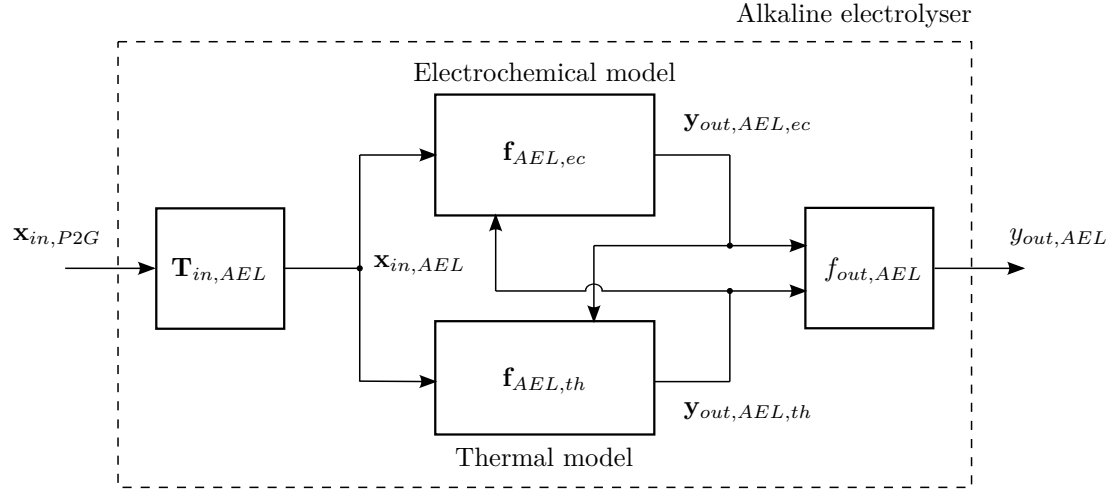
Figure 3.4.: Structure, in- and outputs of the alkaline electrolyser model

and into a thermal model with the output

$$
\begin{aligned}
\mathbf{y}_{out,AEL,th} &= \mathbf{f}_{AEL,th}(\mathbf{x}_{in,AEL}, \mathbf{y}_{out,AEL,ec}) \\
&= \left[T, \dot{Q}_{cool} \right]^T .
\end{aligned}
\tag{3.23}
$$

With the output function

$$
f_{out,AEL} = \begin{bmatrix} 0 & 0 & 1 & 0 \end{bmatrix} \mathbf{y}_{out,AEL,ec} + \begin{bmatrix} 0 & 0 \end{bmatrix} \mathbf{y}_{out,AEL,th}
\tag{3.24}
$$

the electrolysers output

$$
y_{out,AEL} = \dot{V}_{H_2}.
\tag{3.25}
$$

The two submodels influence each other, e.g. a higher production of hydrogen results in an increasing electrolyser temperature. A raising electrolyser temperature decreases the electrolyser's voltage. The electrochemical model describes the relationship of electrical input power, produced hydrogen and efficiency of the electrolyser. The thermal model calculates the electrolyser's temperature and the cooling demand, depending on efficiency.

3.1.3. Electrochemical Model

The voltage of one cell U_{cell} is formed by

- the voltages of anode and cathode,
- the ohmic voltage losses,
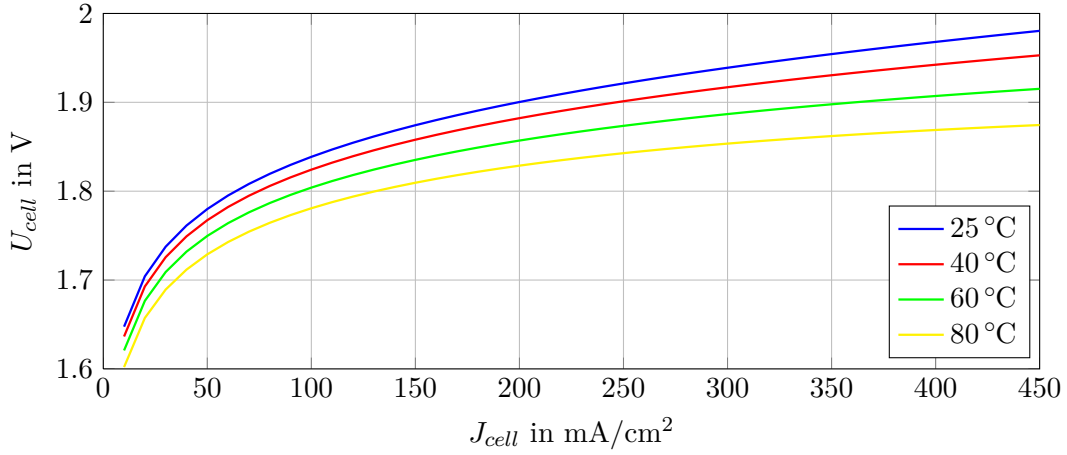
Figure 3.5.: Model's cell voltage over the cell current density for different temperatures ϑ and a system pressure $p = 10\,\text{bar}$.

- the bubble voltage,

- the diaphragm voltage and

- the electrolyte voltage.

According to [49] electrode kinetics of one AEL cell can be modelled by a current-voltage relationship

$$U_{cell}(p,T) = U_{rev}(p,T) + \frac{r_1 + r_2\,\vartheta}{A}\,I_{cell} + s\,\log\left(\frac{t_1 + \frac{t_2}{\vartheta} + \frac{t_3}{\vartheta^2}}{A}\,I_{cell} + 1\right) \qquad (3.26)$$

with ϑ the temperature T in °C with the conversion $\vartheta = T - 273.15$. Equation (3.26) describes the temperature efficiency of the ohmic resistance parameter r_1, r_2 and the overvoltage parameters s, t_1, t_2, t_3. The cell voltage's parameters are listed in Table A.1. The relationship between the current density

$$J_{cell} = I_{cell}/A \qquad (3.27)$$

and U_{cell} of (3.26) depending on the electrolyser's temperatures with $\vartheta \in \{25,40,60,80\}$°C is shown in Figure 3.5. It is noticeable that the cell voltage is decreasing with increasing temperature at a constant value of current density. An electrolyser stack consists of N_S serial cells, building the stack with the overall electrolyser voltage that equals

$$U_{AEL} = U_{stack} = N_S\,U_{cell} \qquad (3.28)$$

is called as stack voltage. The electrolyser consists of N_P parallel stacks, which contribute to the overall electrolyser current

$$I_{AEL} = N_P\,I_{stack} = N_P\,i_{cell}. \qquad (3.29)$$

Electrochemical Model
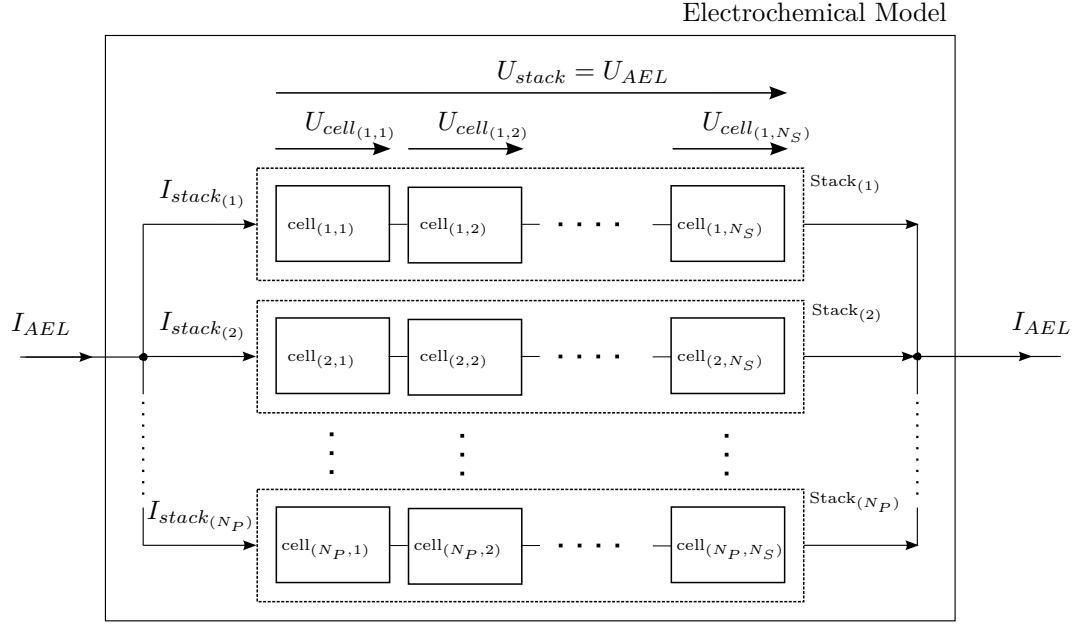
Figure 3.6.: Electrical model of the electrolyser, consisting of N_S serial cells per stack and N_P parallel stacks

Therefore the electrolyser consists of

$$N_{cell} = N_S \ N_P \tag{3.30}$$

electrolyser cells as shown in Figure 3.6. This model is completely scalable with respect to the nominal power of the electrolyser, by varying N_S and N_P. Usually N_S stays constant and defines a 1 MW stack[1]. N_P scales the plant up to $n1$ MW and results in $N_P = n$.

As shown in (3.26) the cell voltage of an electrolyser consists of the system pressure p and the system temperature T. The system pressure is pre-defined[2] and stays constant during simulation. System temperature will be calculated by the thermal model in 3.1.4. The reversible cell voltage $U_{rev}(p,T)$ is pressure and temperature dependent as well.

The temperature

$$\left(\frac{\partial U_{rev}(p,T)}{\partial T}\right)_{p=const} = -\frac{1}{z \ F} \left(\frac{\partial \Delta G(p,T)}{\partial T}\right)_{p=const}$$
$$= \frac{\Delta S(p,T)}{z \ F} \tag{3.31}$$

---

[1] At the nominal parameters $U_{stack} = 135.5$ V, $\vartheta = 75\,°C$.

[2] The system pressure of the following chapters is 7 bar.

and pressure changes

$$\left(\frac{\partial U_{rev}(p,T)}{\partial p}\right)_{T=const} = -\frac{1}{z\ F}\left(\frac{\partial \Delta G(p,T)}{\partial T}\right)_{T=const}$$
$$= \frac{\Delta V(p,T)}{z\ F} \tag{3.32}$$

of [41] can be approximated. ΔV of (3.32) is the change of gas volume caused by a variation of pressure. A very good approximation of pressure and temperature dependence of reversible voltage

$$U_{rev}(p,T) = \underbrace{\left(\frac{\partial U_{rev}(p,T)}{\partial T}\right)_{p=p_{std}}}_{=U_{rev,T}} + \underbrace{\frac{R\ \vartheta}{z\ F}\ \ln\left(\frac{(p-p_{v,KOH}(T))(p-p_{v,KOH}(T))^{0.5}}{a_{\mathrm{H_2O},KOH}(T)}\right)}_{=U_{rev,p}} \tag{3.33}$$

is published in [51] and [32]. Equation (3.33) consists of an approximated temperature dependent

$$U_{rev,T} \approx u_1 + u_2\ \vartheta + u_3\ \vartheta \ln(\vartheta) + u_4\ \vartheta^2 \tag{3.34}$$

and a pressure dependent term $U_{rev,p}$. The pressure dependent term $U_{rev,p}$ of [51] includes the vapour pressure of the KOH solution

$$p_{v,KOH}(T) = \exp(a_1 + a_2 \ln(p_{v,\mathrm{H_2O}})) \tag{3.35}$$

with

$$a_1 = \begin{bmatrix} a_{1,1} & a_{1,2} & a_{1,3} \end{bmatrix} \begin{bmatrix} m \\ m^2 \\ m^3 \end{bmatrix}, \tag{3.36}$$

$$a_2 = a_{2,0} + \begin{bmatrix} a_{2,1} & a_{2,2} & a_{2,3} \end{bmatrix} \begin{bmatrix} m \\ m^2 \\ m^3 \end{bmatrix}, \tag{3.37}$$

and the vapour pressure of pure water

$$p_{v,\mathrm{H_2O}}(T) = \exp\left(b_1 - \frac{b_2}{\vartheta} - b_3\ \ln(\vartheta) + b_4\ \vartheta\right) \tag{3.38}$$

with molal concentration of 30% wt. KOH solution $m = 7.64\,\mathrm{mol\,kg^{-1}}$. The water activity

$$a_{\mathrm{H_2O},KOH}(T) = \exp\left(c_1\ m + c_2\ m^2 + \frac{c_3\ m + c_4\ m^2}{\vartheta}\right) \tag{3.39}$$

of the KOH solution is temperature dependent [51]. The parameter values used in (3.34)-(3.39) are listed in Tables A.2 to A.6.

Faraday efficiency

$$\eta_F = \frac{\left(\frac{i_{cell}}{A}\right)^2}{f_1 + \left(\frac{i_{cell}}{A}\right)^2} \; f_2 = \frac{j_{cell}^2}{f_1 + j_{cell}^2} \; f_2 \tag{3.40}$$

of an electrolyser expresses the amount of electrical energy used for hydrogen production. Parasitic current losses through the gas pipes cause a reduction of Faraday efficiency. Therefore it is called current efficiency [49]. The used Faraday efficiency parameters f_1 and f_2 of (3.40) are derived from the project PHOEBUS. It was a stand-alone PV-hydrogen energy plant in Jülich, Germany for research purposes [35]. The parameters resulting of the PHOEBUS experiment are given in Table A.7.

The hydrogen production

$$\dot{n}_{\text{H}_2} = \eta_F \frac{N_S \; N_P}{z \; F} \tag{3.41}$$

and oxygen production

$$\dot{n}_{O_2} = \frac{\dot{n}_{\text{H}_2}}{2} = \eta_F \frac{N_S \; N_P}{2 \; z \; F} \tag{3.42}$$

rate can be described using the Faraday efficiency [49]. The volume rate

$$\dot{V}_{\text{H}_2} = \dot{n}_{\text{H}_2} \; V_{std} \;\; \text{and} \;\; \dot{V}_{O_2} = \dot{n}_{\text{H}_2} \; V_{std} \tag{3.43}$$

results in the multiplication of the production rate with the volume of an ideal gas at standard conditions $V_{std} = 0.0224 \, \text{m}^3/\text{mol}$. Figure 3.7 shows the hydrogen production curve with the power input of a typical PV plant.

The production of heat as a by-product in an electrolyser results by electrical ineffi-ciencies. The energy efficiency[3]

$$\eta_e = \frac{U_{th}}{U_{cell}} \tag{3.44}$$

results from the thermoneutral voltage (3.19) to the cell voltage (3.26). With an increasing cell voltage the hydrogen production (3.41) increases but the energy efficiency decreases. The efficiency of an alkaline electrolyser depends on the input power P_{P2G}. An increasing input power results in a lower efficiency.

---

[3]only valid without auxiliary heaters

Figure 3.8 shows the efficiency in dependence of the input power at a constant temperature. This curve fits very well to the efficiency of commercial electrolysers of [19]. The input power starts at 20% of nominal power, because AEL usually operates above standby power. If the AEL input power is below 20% it has to be shut down and it takes about $30 - 60$ min until the electrolyser is switched on again [50]. The time is needed to purify the AEL with nitrogen [44],[50].

In the case the AEL electrolyser works at least at standby power, the electrolyser is capable to operate with dynamic input power [44]. For that reason AEL electrolysers are rarely shut-down, but work at standby power. This standby power is about 10-20% of nominal power. This standby power is needed to supply the AEL's auxiliary equipment[11], e.g. heaters, heat exchangers, gas driers, pumps and deoxidisers.

The auxiliary equipment is not a part of the AEL model presented in this chapter. For that reason the AEL model used in the Chapter 5 is expanded. The AEL's expansion expresses in the stop of H_2 production if the standby power is reached or dropped. In that case the input power is used to supply the auxiliary equipment.

To conclude the description of the electrochemical model the output of the electrochemical model $\mathbf{f}_{AEL,ec}$ can be written as

$$\mathbf{y}_{out,AEL,ec} = \mathbf{f}_{AEL,ec}(\mathbf{x}_{in,AEL}, \mathbf{y}_{out,AEL,th}) = \begin{bmatrix} N_S \ U_{cell} \\[1em] \dfrac{P_{P2G} \ \eta_{AC/DC}}{U_{AEL}} \\[1em] \eta_F \dfrac{N_S \ N_P}{z \ F} V_{std} \\[1em] \dfrac{U_{th}}{U_{cell}} \end{bmatrix} . \qquad (3.45)$$

3.1.4. Thermal Model

The goal of the thermal model is to determine the electrolyser's temperature. The thermal model of this section is a combination of thermal models presented in [49] and [10]. Figure 3.9 illustrates the in- and output parameters of the model. The thermal model consists of the input parameters of the electrolyser (3.1) and the output parameters of the electrochemical model (3.45). The resulting parameters of the thermal model

$$\begin{aligned} \mathbf{y}_{out,AEL,th} &= \mathbf{f}_{AEL,th}(\mathbf{x}_{in,AEL}, \mathbf{y}_{out,AEL,ec}, \dot{Q}_{cool}) \\ &= \left[T, \dot{Q}_{cool}\right]^T \end{aligned} \qquad (3.46)$$

are temperature, and systems cooling demand. A PI-controller defines the cooling
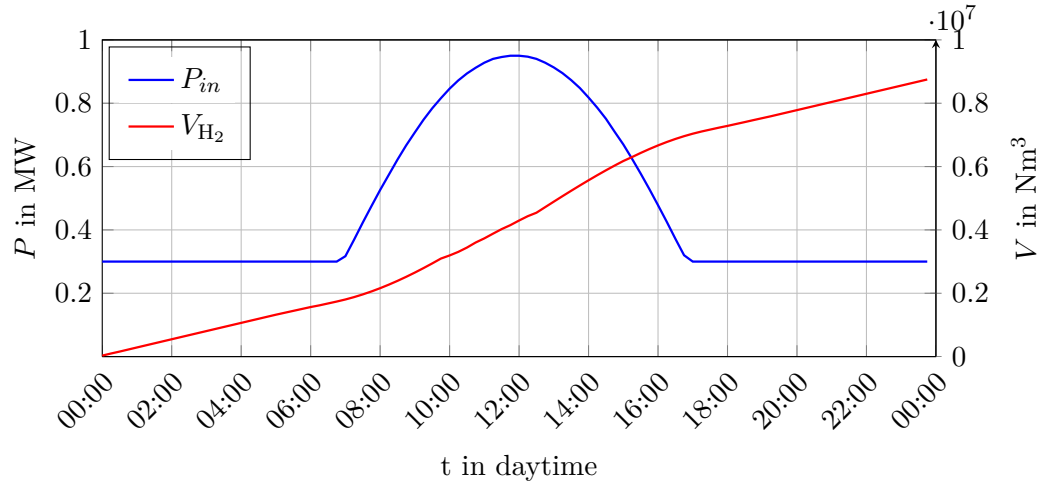
Figure 3.7.: Produced hydrogen in dependence to input power P_in. The input equals the power of a typical PV production.
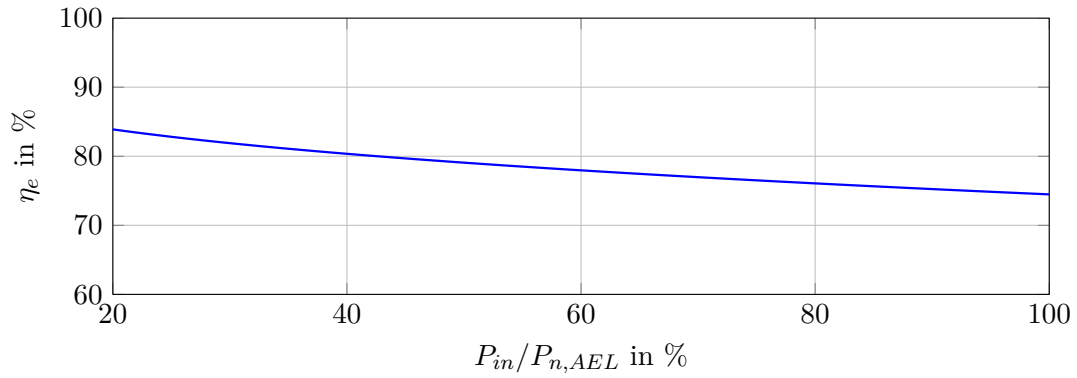
Figure 3.8.: Efficiency of an alkaline electrolyser over the input power. The electrolyser temperature is constant at $\vartheta = 85\,°\mathrm{C}$.

demand

$$\dot{Q}_{cool} = f_{AEL,PI}(\mathbf{y}_{out,AEL,th}, T_{set}) \tag{3.47}$$

depending on the electrolysers temperature T. The time dependence of the electrolysers temperature

$$\frac{dT}{dt} = \dot{T} = \frac{1}{C_T}\left(\dot{Q}_{gen} - \dot{Q}_{loss} - \dot{Q}_{sens} - \dot{Q}_{cool}\right) \tag{3.48}$$

can be modelled as a linear combination of the internal heat generation $\dot{Q}_{gen}$, the heat losses $\dot{Q}_{loss}$, the sensible heat $\dot{Q}_{sens}$, the cooling demand $\dot{Q}_{cool}$ and is indirect proportional

to the thermal capacity C_T [25]. The latent heat leaving the system is neglected in this work.

In order to guarantee a full scaleability of this model the thermal capacity

$$C_T(P_{n,AEL}) = d_0 + d_1 \ P_{n,AEL} \tag{3.49}$$

is a function of the electrolyser's nominal power $P_{n,AEL}$. The parameters d_0 and d_1 are calculated by a linear approximation of the thermal capacities of PHOEBUS[4], HYSOLAR electrolyser [9] and on the information based on the dialog with Hydrogenics and NEL during the Hannover Messe 2013 [37],[24]. They are listed in Table A.8.

A lower electrical efficiency (3.44) increases the internal heat generation

$$\dot{Q}_{gen} = N_S \ N_P \left(u_{cell} - U_{th}\right) i_{cell} = N_S \ N_P \left(1 - \eta_e\right) u_{cell} \ i_{cell} \ . \tag{3.50}$$

of the electrolyser. Heat losses

$$\dot{Q}_{loss} = \frac{1}{R_T} \left(T - T_{ambient}\right) \tag{3.51}$$

can be modelled as a function of the convective heat transfer resistance R_T and the temperature difference between the electrolyser and the ambient [10]. A higher internal temperature results in higher heat losses by radiation, at constant ambient temperature. The thermal time constant

$$\tau_T = R_T \ C_T \tag{3.52}$$

characterises the first order system's time dynamic and is based on R_T and on the thermal capacity (3.49).

The sensible heat

$$\begin{aligned} \dot{Q}_{sens} = &\left(\dot{m}_{H_2,AEL} \ \hat{c}_{p,H_2} + \dot{m}_{O_2,AEL} \ \hat{c}_{p,O_2}\right) \left(T_{cond} - T_{ambient}\right) \\ &+ \dot{m}_{H_2O,AEL} \ \hat{c}_{p,H_2O} \left(T - T_{ambient}\right) \end{aligned} \tag{3.53}$$

is described by following terms
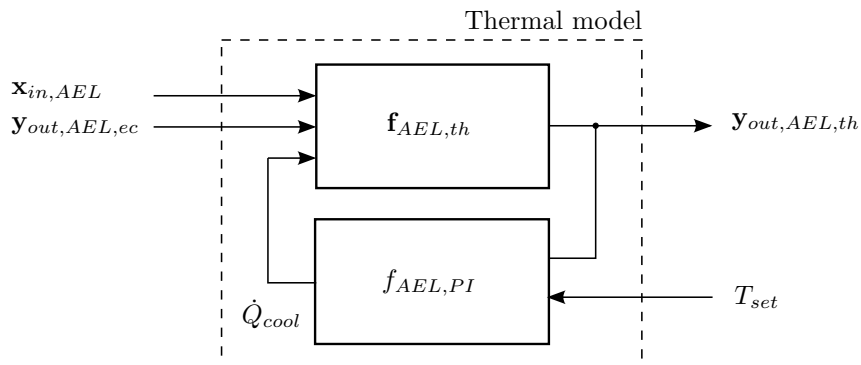
Figure 3.9.: In- and outputs of the thermal model

- the sensible heat taken out of the system by the hydrogen and oxygen flow

- and for the heat required to warm the input water from the ambient temperature up to the electrolyser's internal temperature [10].

The parameter $\hat{c}_{p,X}$ represents the specific heat of an element X at a constant pressure [36]. The mass flow

$$\dot{m}_X = \dot{V}_X \, \rho_{n,X} \tag{3.54}$$

can be calculated with volume flow $\dot{V}_X$ and density $\rho_{n,X}$ of element X. The used density of H_2, O_2 and H_2O are itemised in Table A.9. The last variable of (3.48), the cooling demand $\dot{Q}_{cool}$ is determined by a heat exchanger working with cooling water [49].

The cooling characteristics of an electrolyser with nominal power $P_{n,AEL} > 1\,\text{MW}$ are not published yet. For that reason the maximum cooling power

$$\dot{Q}_{cool,max} = 25\% \, P_{n,AEL} \tag{3.55}$$

is limited, depending linear to nominal power $P_{n,AEL}$. A PI controller according to [29]

$$G_{cont}(s) = \frac{\dot{Q}_{cool}}{\Delta T} = V_P + \frac{V_I}{s} \qquad \Delta T = T - T_{set} \tag{3.56}$$

is used to control the temperature to the aimed value T_{set}. The output of the PI controller $\dot{Q}_{cool}$ results in

$$\dot{Q}_{cool} = f_{AEL,th}(\mathbf{y}_{out,AEL,th}) = V_I \int_0^t \Delta T(\tau)d\tau + V_P \Delta T(t) \, , \qquad T(0) = T_{start} \, . \tag{3.57}$$

The controller parameters are given in Table A.10 and are determined with the frequency response procedure according to [29]. Figure 3.10 shows the temperature step response and the process to heat the electrolyser from the ambient temperature up to operating temperature and the standarised cooling $\dot{q}_{cool} = \dot{Q}_{cool}/P_{n,AEL}$. The warm-up needs about 1.5 to 3 hours until the electrolyser will be preheated and stays in the area of operating temperature until a revision[4]. Standby power is about 10 to 20% of nominal power $P_{n,AEL}$, which prevents the electrolyser of cooling down.

As a conclusion output as a function of the thermal model $\mathbf{f}_{AEL,ec}$ can be written by

$$\mathbf{y}_{out,AEL,th} = \mathbf{f}_{AEL,th}(\mathbf{x}_{in,AEL}, \mathbf{y}_{out,AEL,ec}, \dot{Q}_{cool}) = \begin{bmatrix} T_{start} + \int_0^t \dot{T}(\tau)d\tau \\ \\ \dot{Q}_{cool} \end{bmatrix} . \tag{3.58}$$

---

[4]depending on the AEL type and if an auxiliary heater is installed

3.2. Methanation

Methanation is a standard technology used for coal gasification and developed for biomass gasification [46]. In a P2G plant methanation is used to transform H_2 and CO_2 to methane (CH_4). Reasons [46] to use CH_4 (SNG) instead of H_2 are

- that the natural gas grid allows a wide feed-in and a huge storage capacity and

- the volume reduction by a factor 5:1.

Methanation was found in 1902 by Sabatier and Senderens. The two main applications of the methanation process are

- the removal of CO in hydrogen rich gases and

- the conversion of synthesis gas to synthetic natural gas (SNG) [28].

Three typical reactor types are fixed-bed, fluidised-bed and Slurry Bubble Column Reactor (SBCR). Table 3.3 shows the advantages and disadvantages of these three types. According to [28] conversion can be described by three reactions, the methanation reaction

$$3H_2 + CO \longleftrightarrow CH_4 + H_2O, \quad \Delta H_R^0 = -206.28 \, \text{kJ/mol} , \qquad (3.59)$$

and the water gas shift

$$CO + H_2O \longleftrightarrow CO_2 + H_2, \quad \Delta H_R^0 = -41.16 \, \text{kJ/mol}. \qquad (3.60)$$
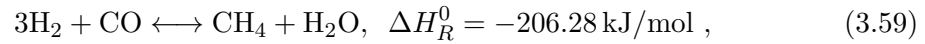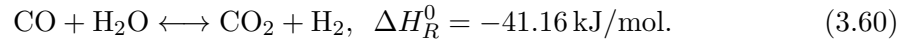
The exothermic reactions (H_R^0 negative) pass through a catalyst build of nickel, platinum, iron or ruthenium. Nickel is the most common material due to financial and technical
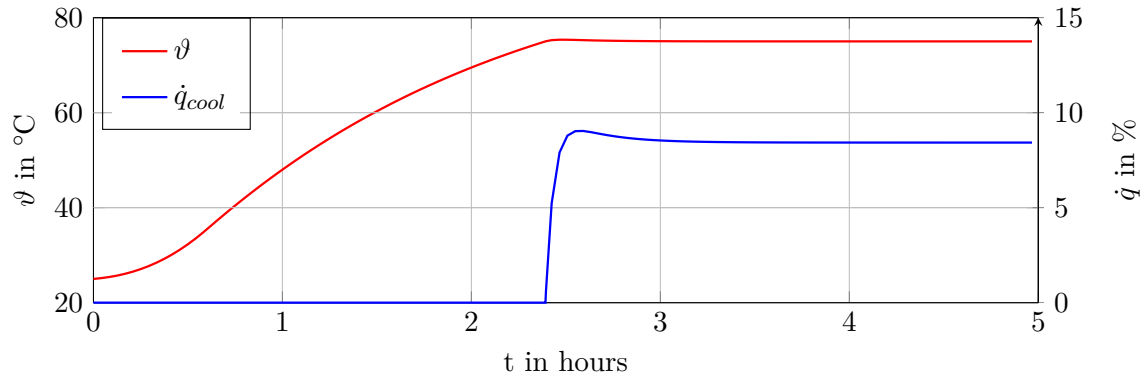
Figure 3.10.: Temperature step response of the AEL electrolyser in red and the blue standardised cooling demand $\dot{q}_{cool}$ required to control the temperature. Starting temperature $\vartheta_{start} = 25\,°C$.

Table 3.3.: Comparison of reactor types for methanation according to [21]

	Fixed-bed	**Fluidised-bed**	**SBCR**
Advantages	Low mechanical load on catalyst	Effective heat removal	Very effective heat removal
	Wide range of operation	Small temperature gradients	Isothermal conditions
	Simple catalyst handling	Good mass transfer	Less sensitive to fluctuating feed stream
	Simple dimension and up scaling	Only one reactor necessary	Only one reactor necessary
			No heat exchanger inside the reactor
Disadvantages	Removal of heat	High mechanical load on catalyst	Liquid-side mass transfer limitations possible
	Temperature gradients	Entrainment of catalyst	Backmixing possible
	Multiple reactors in series		Evaporation and decomposition of heat transfer liquid
	Mass transfer limitation due to particle size possible		

advantages [28]. By linear combination of the reactions (3.59) and (3.60) the following reaction

$$4H_2 + CO_2 \longleftrightarrow CH_4 + 2H_2O, \quad \Delta H_R^0 = -165.12\,\text{kJ/mol} \qquad (3.61)$$
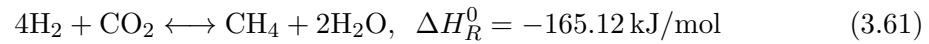
can be formed. Too high temperatures and the availability of steam can lead to a methane reformation by the reactions (3.59) and (3.61) of methane and steam back to hydrogen with carbon monoxide or carbon dioxide. To avoid methane reformation, prevention of temperature peaks is necessary.[20]

According to [46] possible CO_2 sources are

- direct capture of CO_2 from the air,

- integration in biogas or biomas gasification plants,

- integration in sewage plants, landfill sits and CO_2-intensive industry and

- integration in fossil fueled power plants.

It is assumed that the CO_2 source is available for both representative model regions and requires no further consideration.
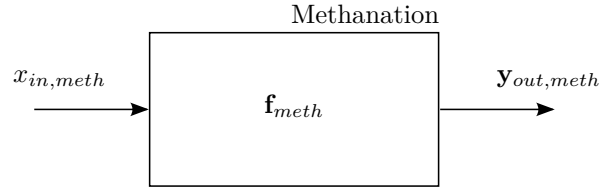
Figure 3.11.: In- and output of the methanation model

The main focus of this work lies in the investigation of the interface between the electrical grid - P2G plant. Due to this fact the model of the methanation is held very simple. A pure CO_2 methanation is not yet state-of-the-art and is currently under research [46]. No measurements and data of a CO_2 methanation unit were found during the literature phase of this work. The electrolyser dynamics, as first element of the P2G plant, determines the input characteristics of the P2G plant and the methanation is only seen as a simple conversion of H_2 and CO_2 to CH_4. The input of methanation

$$x_{in,meth} = y_{out,AEL} = \dot{V}_{H_2} \tag{3.62}$$

is the electrolyser's output, as shown in Figure 3.11. The methanation's output

$$\begin{aligned} \mathbf{y}_{out,meth} &= \mathbf{f}_{meth}(\mathbf{x}_{in,meth}) \\ &= \left[\dot{V}_{CH_4,meth}, \dot{V}_{H_2O,meth}, \dot{V}_{CO_2,meth} \right]^T \end{aligned} \tag{3.63}$$

provides following variables, of the flow rate of produced methan $\dot{V}_{CH_4,meth}$, the flow rate of produced water $\dot{V}_{H_2O,meth}$ and the flow rate of required CO_2, $\dot{V}_{CO_2,meth}$.

The amount of substance

$$n_X = \frac{V}{V_{std}} \tag{3.64}$$

of the element X is calculated with the molar volume at standard conditions V_{std}. The output of the methanation according to equation (3.61) is

$$\begin{aligned} \mathbf{y}_{out,meth} &= \mathbf{f}_{meth}(\mathbf{x}_{in,meth}) \\ &= \underbrace{\begin{bmatrix} 1/4 & 0 & 0 \\ 0 & 1/2 & 0 \\ 0 & 0 & 1/4 \end{bmatrix}}_{\mathbf{T}_{meth}} \frac{\dot{V}_{H_2}}{V_{standard}}. \end{aligned} \tag{3.65}$$

with the stoichiometric matrix $\mathbf{T}_{meth}$[34]. The heat produced by the methanation is not investigated in this work.

4. Representative Electrical Grid Models

In this chapter two representative distribution grids of the middle voltage level, that are used for the investigation of the P2G operation strategies, are described. These two grids are adopted from the masterthesis of O. Oberzaucher [38]. First representative describes a grid in a rural region with agricultural and private household. The second grid represents a suburban region with only private households. The assumption of this work is that every private as well as agricultural household have installed PV plant. A P2G plant in each of the two grids transforms the surplus of renewable energy in chemical energy. The feed-in of SNG in the natural gas grid is not an issue of this work.

4.1. Grid Topologies

Figure 4.1 shows the topology of the rural grid and Figure 4.3 shows the suburban grid. Simulating the high voltage grid is not a part of this work. The high voltage grid provides power for the distribution level, if the renewable energy sources in the distribution grids do not produce enough electrical power. The two grids include a P2G plant. In the rural grid the P2G plant is near the transformer and in the suburban grid in the grid's middle. By comparing these two grids it is obvious that the rural grid shows a higher amount of nodes and lines. The rural grid also includes a windpower plant labelled by WP. The transformer represents the gateway to the high voltage grid. The two grids are implemented by PSS®Sincal and the grid parameters are adopted from [38] as well and listed in the Appendix Sections A.3 and A.4. The used load profiles [27] of a private household and of an agriculture are specified in Section 4.2 together with the used PV and WP profiles.

The loads illustrated in the Figures 4.1 and 4.3 represent the residual load of a defined number of private households and agricultures. This load consists of a secondary substation and the residual load of private households, agricultures and the PV power plant at the roof of every household. The rural grid includes agricultures and private households as shown in Figure 4.2, while the suburban grid only includes private households illustrated by Figure 4.4.

4.1.1. Rural Grid

The rural grid in Figure 4.1 represents a typical wide grid structure with a low population density. It's a radial spread grid with four radial branches which are splitting in further. The grid works as an open half ring. This means that if a line goes out of service, the the ring gets closed and the energy supply will be ensured from the other side. The reliability
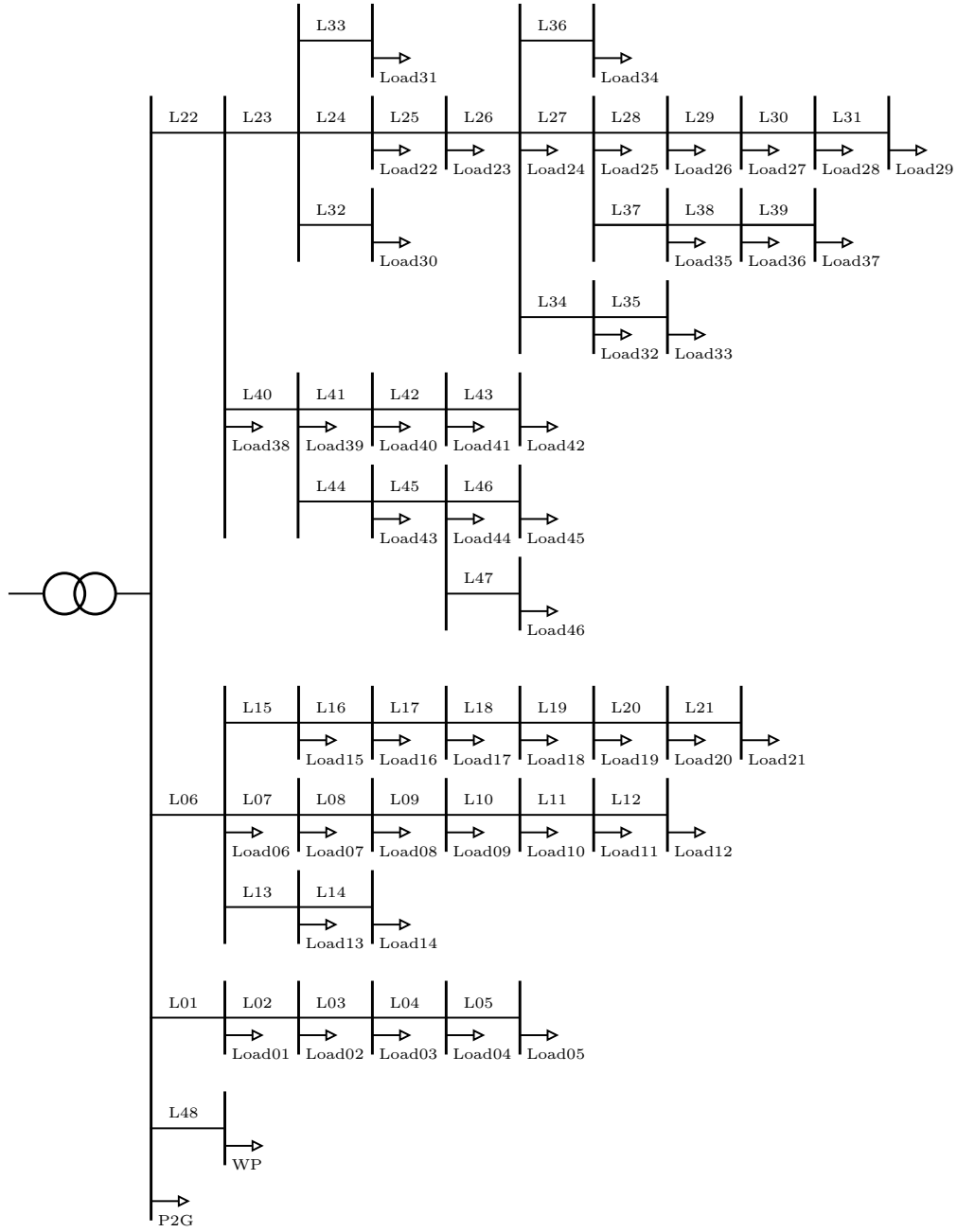
Figure 4.1.: Topology of an rural grid. It consists of 46 loads, a P2G plant and a wind farm. Picture based on [38]
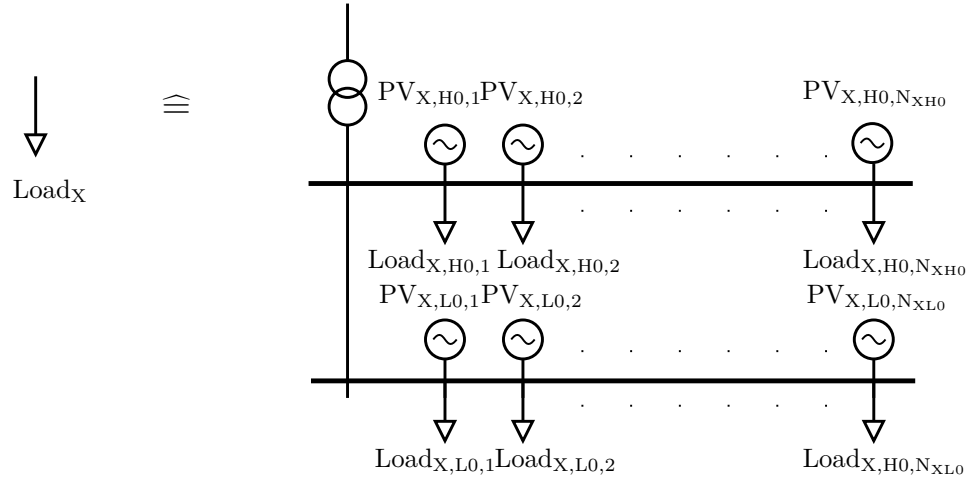
Figure 4.2.: One load in the rural grid consists of a secondary substation, $N_{\mathrm{X}H0}$ private households and $N_{\mathrm{X}L0}$ agricultures

analysis is not a part of this work.

The parameters of the grid

- load values,

- line types and length

are listed in Tables A.11-A.13.

As mentioned in 4.1 and shown in Figure 4.2 one load only symbolises a certain number of private households and agricultures. The private households are represented by the $H0$ profiles and the agricultures by the $L0$ profiles, described in Section 4.2. In order to calculate the number of households $N_{\mathrm{X}H0}$ and the number of agricultures $N_{\mathrm{X}L0}$ of a load, the installed power, of a private household

$$P_{H0} = 2\,\mathrm{kW} \tag{4.1}$$

and of an agriculture

$$P_{L0} = 15\,\mathrm{kW} \tag{4.2}$$

was used. A part of the aDSM study [22] describes a virtual settlement which reflects the housing conditions in Austria. Based on the results of [22] and [38] a representative installed power for a rural region built of 90% private households and 10% agricultures, installed power is calculated by

$$\bar{P}_{rural} = 90\%P_{H0} + 10\%P_{L0} = 3.3\,\mathrm{kW}. \tag{4.3}$$

The total number of households and agricultures of a load with the index $X \in \{1,2,\ldots,46\}$

$$N_{Xtotal} = \frac{S_{load,X}}{\bar{P}_{rural}} \tag{4.4}$$

consists of

$$N_{XH0} = 90\% N_{Xtotal} \tag{4.5}$$

and

$$N_{XL0} = 10\% N_{Xtotal}. \tag{4.6}$$

The values of $S_{load,X}$ in (4.4) are listed up in Table A.12. The total number of private households in the rural grid

$$N_{H0} = \sum_{X=1}^{46} N_{XH0} = 2231 \tag{4.7}$$

and the total number of agricultures

$$N_{H0} = \sum_{X=1}^{46} N_{XL0} = 248. \tag{4.8}$$

The study [33] investigated the roof PV potential of Bavaria and Germany. Due to the fact that the area and grid infrastructure of Bavaria is very similar to Austria, this PV potential is used in this work. According to this study [33] the potential of a private household in a rural area is defined as

$$\hat{P}_{PV,H0,rural} = 13.7 \, \text{kWp/Household} \tag{4.9}$$

and of a farm

$$\hat{P}_{PV,L0} = 53.9 \, \text{kWp/Household}. \tag{4.10}$$

Since the area of an agriculture roof is bigger than the roof are of a private household, the PV potential is higher, as well.
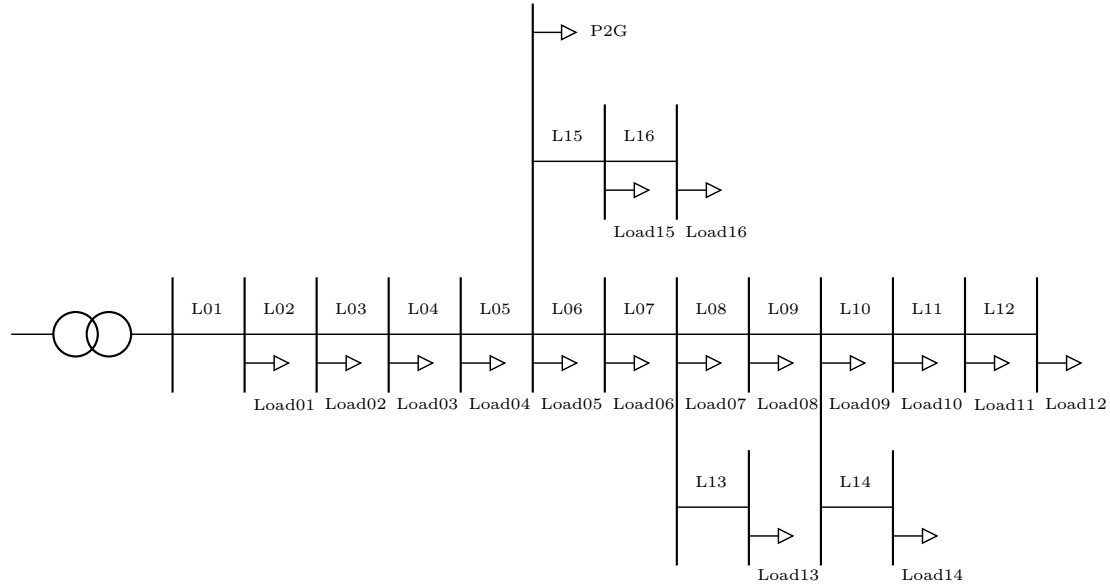
Figure 4.3.: Topology of a suburban grid. Picture based on [38]

4.1.2. Suburban Grid

The suburban grid illustrated in Figure 4.3 is a representative grid close to a city with high people density. The grid structure is an open half-ring like the rural grid too. If disturbances on a line occur energy supply can be guaranteed by closing the open ring on the other side. The load is defined by private households, because no agricultures are available in a suburban area and any other electrical consumers e.g. industry are neglected. The grid parameters and data are elicited in the Tables A.14-A.16. Figure 4.4 shows the residual load the suburban grid. The residual load consists of a defined number of private household represented by the profile $H0$ and a PV plant on the roof of each household. The calculation of the number of households of a load with the index $X \in \{1,2,\ldots,16\}$ by

$$N_{XH0} = \frac{S_{load,X}}{P_{H0}} \tag{4.11}$$

with P_{H0} of (4.1) is easier than in the rural grid. The values of $S_{load,X}$ are listed in Table A.15. The total number of private households

$$N_{H0} = \sum_{X=1}^{16} N_{XH0} = 1600. \tag{4.12}$$

The roof PV potential according to [33] is

$$\hat{P}_{PV,H0,suburban} = 8.7\,\text{kWp/Household}. \tag{4.13}$$

The smaller PV potential per household in the suburban area in comparison to the rural area is explainable with lower available roof area per household.
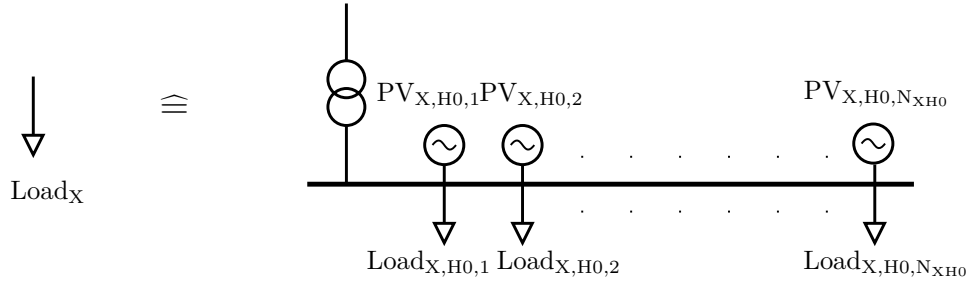
Figure 4.4.: One load in the suburban grid consists of a local power transformer and $N_{\mathrm{X}H0}$ private households

4.2. Profiles

This section describes load, PV and WP profiles used for load flow calculations in the rural and suburban grid. The load profiles indicate the power consumption of different groups of energy consumers over the day, depending on weekday and season. The PV and WP profiles describe the electrical power generation of PV and WP plants depending on day and season.

4.2.1. Load Profiles

Distribution grid operating companies use defined load profiles like [27] to calculate the balancing energy. According to [3] standardised load profiles are:

> "In order to forecast balance groups' balancing energy demand it is necessary to have actual consumption data, acquired by load profile meters. However, the technical and administrative costs involved in providing small consumers with load profile meters would be inordinate, so standardised load profiles are assigned to this consumer group. The suppliers' schedules are derived from these load profiles."

The sampling time of the used profiles is 15 min. In this work load profiles are used to define the demand during simulation period. The standardised load profile of a private household with an energy consumption of

$$E_{H0} = 1000\,\mathrm{kWh/a} \tag{4.14}$$

is called $H0$ and an agriculture with a energy consumption of

$$E_{L0} = 1000\,\mathrm{kWh/a} \tag{4.15}$$

is called $L0$ profile [27]. According to [45] the average electrical energy consumption of a private household is

$$\bar{E}_{H0} = 4000\,\text{kWh/a} \tag{4.16}$$

and of an agriculture is

$$\bar{E}_{L0} = 16\,000\,\text{kWh/a}. \tag{4.17}$$

Therefore the standardised load $H0$ profile is multiplied with a factor 4 and the $L0$ profile with a factor 16. The scaled $H0$ profile is shown in Figure 4.5 and the scaled $L0$ in Figure 4.6. This Figures illustrate the power consumption of a day, depending on weekday (we, sa, so) and seasons (summer, winter, transitional period).
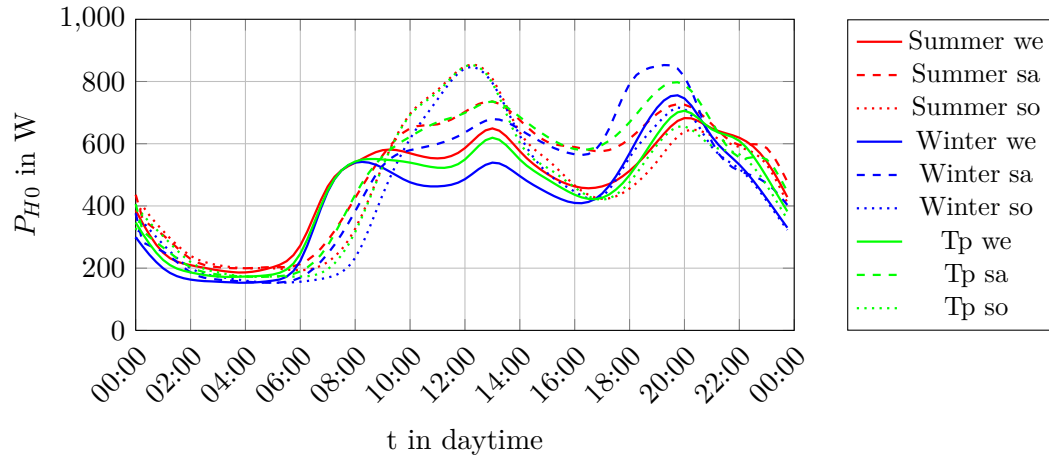
Figure 4.5.: The H0 profile in summer, winter and transition period (Tp)
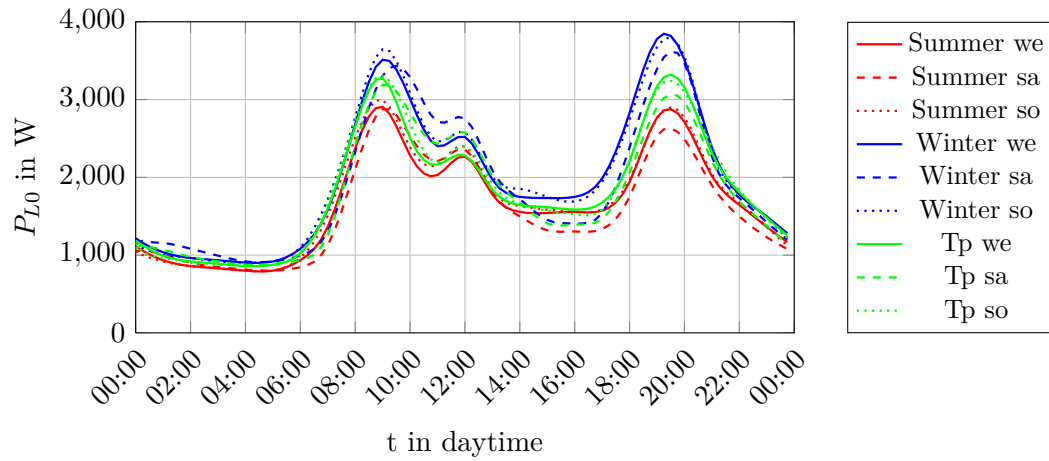
Figure 4.6.: The L0 profile in summer, winter and transition period (Tp)

4.2.2. Photovoltaic Profiles
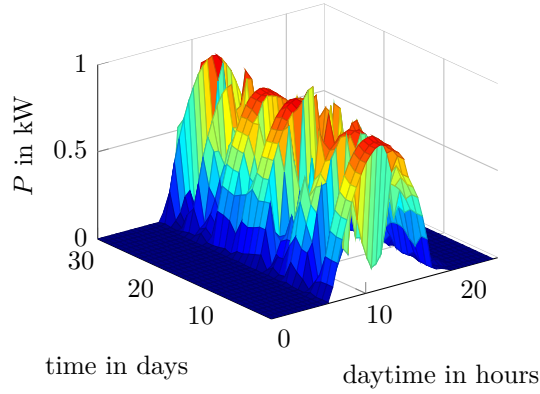
Figure 4.7.: Plot of the PV power production in August
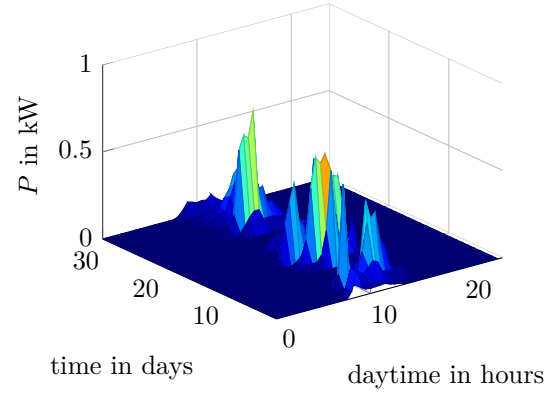
Figure 4.8.: Plot of the PV power production January

In difference to the load profiles it is not possible to use standardised profiles for the PV too. The problem is the simultaneity of weather events[1] and the small area of the model with distribution grid. These weather events influence the PV power production. The rural grid area is rectangle with the estimation of this area equals to

$$A_{rural} \approx \underbrace{\sum_{i=22}^{31} l_{line,i}}_{a} \underbrace{\sum_{j=1}^{5} l_{line,j}}_{b} = 10.8\,\mathrm{km}\ 2.7\,\mathrm{km} = 29.16\,\mathrm{km}^2. \tag{4.18}$$

The assumption is based on the following idea: a is the longest continuous line in the grid and b the shortest. The suburban grid area is an ellipse with the the estimation of this area to

$$A_{suburban} \approx \pi \underbrace{\frac{1}{2} \sum_{i=1}^{12} l_{line,i}}_{c} \underbrace{\frac{1}{2} \sum_{j=13}^{16} l_{line,j}}_{d} = \pi\ 2.15\,\mathrm{km}\ 0.9\,\mathrm{km} = 6.08\,\mathrm{km}^2. \tag{4.19}$$

It is assumed that c is the length of the grid and d is the width. If for example a cloud covers both areas (4.18) and (4.19) the PV power production follows the decreased sun radiation and decreases too. Due to this circumstance it is not possible to use a standardised PV profil because the diversity would be lost. Another important feature is the volatility of alternative energy plants like PV.

The used PV power trends are recorded from a PV plant placed at the roof of the University of Technology in Vienna. The used representative months of the measured

---

[1]especially cloud movements over a fix point

Table 4.1.: Duration in month and days of winter, summer and transition period in the year 2012

	Winter	Transition period	Summer	Σ
Month	3	6	3	**12**
Months	01,02,12	03,04,05,09,10,11	06,07,08	**12**
Sum of days	90	183	92	**365**

date were April (tp), August (summer) 2012 and January (winter) 2013. The measuring resolution of the recorded power is one data point per minute. The step size of the simulation of this work is 15 min. Due to this fact the data points are filtered by an average filter to reduce the sampling time. Figure 4.7 and 4.8 show the energy difference of a summer to a winter month. The power curves are normed to 1 kW for a better scaling. The normed power of one day is

$$p_{PV}(i) \in \mathbb{P}_{PV}, \quad \mathbb{P}_{PV} = \{p \in \mathbb{R} | 0 \leq p \leq 1\,\text{kW}\} \quad \text{for} \quad i \in \{1,2,\dots 96\} \quad (4.20)$$

includes 96 power values and the average energy of a month

$$\bar{E} = \sum_{j=1}^{\text{days}} \underbrace{\int_0^{24} P_j(\tau)d\tau}_{\approx \sum_i^{96} p_{PV}(i)\ 0.25\,\text{h}} \quad , \quad \text{days} \in \{30,31\} \quad (4.21)$$

of the normed PV energy production in the summer, winter and transition period is

$$\bar{E}_{PV,winter} = 15.30\,\text{kWh/month}, \quad (4.22)$$

$$\bar{E}_{PV,summer} = 143.1\,\text{kWh/month and} \quad (4.23)$$

$$\bar{E}_{PV,Tp} = 132.6\,\text{kWh/month}. \quad (4.24)$$

This three months are used for the further combined simulation. In this simulation the yearly results are extrapolated by counting the simulation's outputs of the summer and winter months each three times and of the transitional period six times. To calculate the energy per year of a 1 kW PV plant the energy of the whole winter, summer and transition period with Table 4.1 is

$$E_{PV,winter} = \bar{E}_{PV,winter}\ 12\,\text{month/a}\ \frac{90}{365} = 45.27\,\text{kWh/a}, \quad (4.25)$$

$$E_{PV,summer} = \bar{E}_{PV,summer}\ 12\,\text{month/a}\ \frac{92}{365} = 432.83\,\text{kWh/a and} \quad (4.26)$$

$$E_{PV,Tp} = \bar{E}_{PV,Tp}\ 12\,\text{month/a}\ \frac{183}{365} = 797.78\,\text{kWh/a}. \quad (4.27)$$
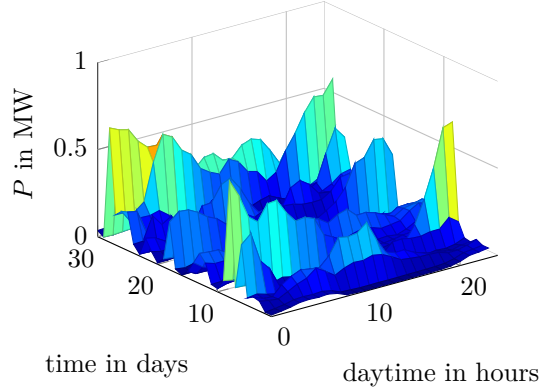
Figure 4.9.: Plot of the WP production in August
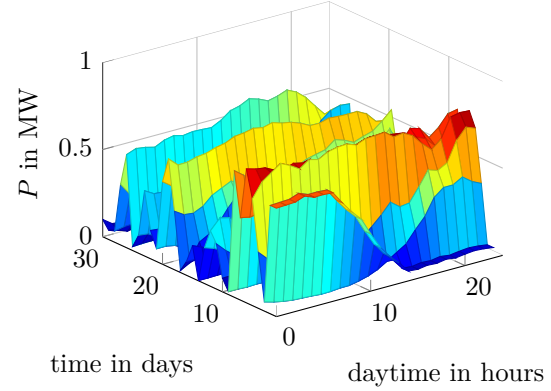
Figure 4.10.: Plot of the WP production in January

The extrapolated yearly result[2] of energy production

$$E_{PV} = E_{PV,winter} + E_{PV,summer} + E_{PV,Tp} = 1276 \, \text{kWh/a} \tag{4.28}$$

equals

$$t_{PV} = \frac{E_{PV}}{1 \, \text{kW}} = 1276 \, \text{h/a} \, . \tag{4.29}$$

t_{PV} is defined as the full load hours per year.

4.2.3. Wind Power Profiles

The rural grid includes a wind farm. The power production profiles of the wind farm "Haindorf-Inning" between Melk and St. Pölten in Lower Austria are used for the simulation [53]. The wind farm consists of seven Enercon WP plants with a nominal power of 1.8 MW per power plant [47]. The power production of the seven WP plant is summed up and normed to a 1 MW WP plant. The result of the normed power of one day

$$p_{WP}(i) \in \mathbb{P}_{WP}, \quad \mathbb{P}_{PV} = \{p \in \mathbb{R} | 0 \le p \le 1 \, \text{MW}\} \quad \text{for} \quad i \in \{1, 2, \dots 96\} \tag{4.30}$$

includes 96 power values.

Figures 4.9 and 4.10 illustrates the difference between the electricity production of a typical summer month and a typical winter month. In contrast to the PV production in Figure 4.7 and 4.8, WP typically produce electrical energy in the winter months. So it is an optimal addition to PV production for a consistent regenerative energy supply.

---

[2]merely an estimation, because the yearly results are extrapolated by three months

Another difference between the WP and PV are the power peaks. The power peaks of PV power production are usually occurring at midday while the WP production is quite constant during the day and night but variable from day to day.

According to calculation (4.21) the of the average energy per month is

$$\bar{E}_{WP,winter} = 15.30 \, \text{kWh/month}, \tag{4.31}$$

$$\bar{E}_{WP,summer} = 143.1 \, \text{kWh/month and} \tag{4.32}$$

$$\bar{E}_{WP,Tp} = 132.6 \, \text{kWh/month}. \tag{4.33}$$

The energy production of periods winter, summer and transition period considering the data of Table 4.1

$$E_{WP,winter} = \bar{E}_{WP,winter} \, 12 \, \text{month/a} \, \frac{90}{365} = 535.27 \, \text{MWh/a}, \tag{4.34}$$

$$E_{WP,summer} = \bar{E}_{WP,summer} \, 12 \, \text{month/a} \, \frac{92}{365} = 206.3 \, \text{MWh/a and} \tag{4.35}$$

$$E_{WP,Tp} = \bar{E}_{WP,Tp} \, 12 \, \text{month/a} \, \frac{183}{365} = 863.24 \, \text{MWh/a}. \tag{4.36}$$

Summing up the above calculated energy production, the yearly energy production[3] is extrapolated by

$$E_{WP} = E_{WP,winter} + E_{WP,summer} + E_{WP,Tp} = 1604.8 \, \text{MWh/a} \tag{4.37}$$

and equals

$$t_{WP} = \frac{E_{WP}}{1 \, \text{MW}} = 1604.8 \, \text{h/a} \, . \tag{4.38}$$

Only the rural grid includes a WP plant. Similar to the project SYMBIOSE[6] the nominal power the WP farm in the rural region is set to $P_{n,WP} = 9 \, \text{MW}$ and the discussed power profile is multiplied therefore with a factor of 9.

---

[3]merely an estimation, because the yearly results are extrapolated by three months

5. Combined Simulation

This chapter discusses the combined simulation of the P2G model (described in Chapter 3) and two representative distribution grids (discussed in Chapter 4). The P2G plant represents a load element in these two grids. By alternating the size of the photovoltaic plants and the P2G plant resulting effects are investigated. The optimal P2G plant size at different PV installation levels is examined too.

The combined simulation's aim is to examine the P2G plant's dynamic over the period of a year. In order to reduce the simulation duration the annual results are approximated by three representative months. Chapter 4 already described the P2G plant's position in the grids. The P2G plant is used as a variable load in the grid and operates with the negative residual load. Each grid is analysed, based on two scenarios. The scenarios differ in the level of PV installation. Scenario 1 investigates the maximum installable PV power and scenario 2 the required PV power for the grid's energy autarchy.

On the basis of these two scenarios the optimal size of the P2G plant is investigated. This is done by four graduations. Another part of this chapter examines two different operation modes of the P2G plant. In the first mode the P2G plant operates at least on the standby power[1] [2] and in the second mode the minimum P2G power is increased to the partial load power[3]. It is not possible to operate the P2G plant with power generated by renewable energy sources, because of high volatility of these renewable power plants, the minimum P2G power can not be guaranteed. At the end of this chapter efficiency[4] and full-load-hours of the two operation modes are compared. It is possible to store a part of the surplus energy in a battery and reduce external power consumption with this action. The count of cycles gives an overview of the P2G plant's loading.

Simulation is executed by PSS®Sincal in combination with Matlab®. The grids are implemented and labelled by PSS®Sincal. Matlab® is used to initialise PSS®Sincal database, to control load flow calculations and variable the values of the PV plant sizes and the P2G plant size, as shown in Figure 5.1. The simulation's duration is set by Matlab®. To simulate the period of a month, Matlab® executes 30 or 31 one day simulations[5].

---

[1]As mentioned in Chapter 3 it is not possible to operate the electrolyser below the standby power.

[2]$P_{P2G,min} = P_{standby} = 15\% P_{n,P2G}$

[3]$P_{P2G,min} = P_{partial} = 30\% P_{n,P2G}$

[4]The P2G plant's efficiency of this work is the ratio of SNG's energy density per consumed electrical energy.

[5]Depending on the month length, e.g. January is 31 days and April 30 days long

The grids are simulated over three season typical months. Therefore

- **summer** is represented by the month August 2012,

- **winter** by January 2013 and

- **transitional period** by April 2012.

The regenerative power production data used for these months are described in Section 4.2. An extrapolation of the yearly results is done by counting the results of summer and winter month each three times, and the results of the transitional period six times. This reduces the simulation duration by a factor of 4.

5.1. Load Calculation

A task of the MATLAB® algorithm is the correct assignment of loads. As mentioned in the sections 4.1.1 and 4.1.2 every load represents a number of agricultures and/or private households with PV plants. The value of the rural grid's residual load X is calculated as

$$P_{load,\text{X}} = N_{\text{X}H0}(\underbrace{p_{PV}\,f_{PV,rural,H0}\hat{P}_{PV,H0,rural}}_{P_{PV,H0,rural}} + P_{H0}) + N_{\text{X}L0}(\underbrace{p_{PV}\,f_{PV,rural,L0}\hat{P}_{PV,L0}}_{P_{PV,L0}} + P_{L0})$$

(5.1)

and the residual load X of the suburban grid with only private households as

$$P_{load,\text{X}} = N_{\text{X}H0}(\underbrace{p_{PV}\,f_{PV,suburban}\hat{P}_{PV,H0,suburban}}_{P_{PV,H0,suburban}} + P_{H0}).$$

(5.2)

The factor p_{PV} describes the normalised PV power to $1\,\text{kW}$ described in Section 4.2.2. $\hat{P}_{PV,H0,rural}$, $\hat{P}_{PV,L0}$ and $\hat{P}_{PV,H0,suburban}$ mean the installable PV plant power according to the study [33]. In the study [33] the PV potential in a rural area of a private household is

$$\hat{P}_{PV,H0,rural} = 13.7\,\text{kWp/Household}$$

(5.3)

and of an agriculture

$$\hat{P}_{PV,L0} = 53.9\,\text{kWp/Household}.$$

(5.4)

The PV potential of a private household in a suburban area is

$$\hat{P}_{PV,H0,suburban} = 8.7\,\text{kWp/Household}.$$

(5.5)

The power factors $f_{PV,rural}$ and $f_{PV,suburban}$ scale the PV plants up to the required size referred to the installable power $\hat{P}_{PV,H0,rural}$, $\hat{P}_{PV,L0}$ and $\hat{P}_{PV,H0,suburban}$. For example if $f_{PV,L0} = 50\%$ a PV plant for an agriculture would install with a peak power of
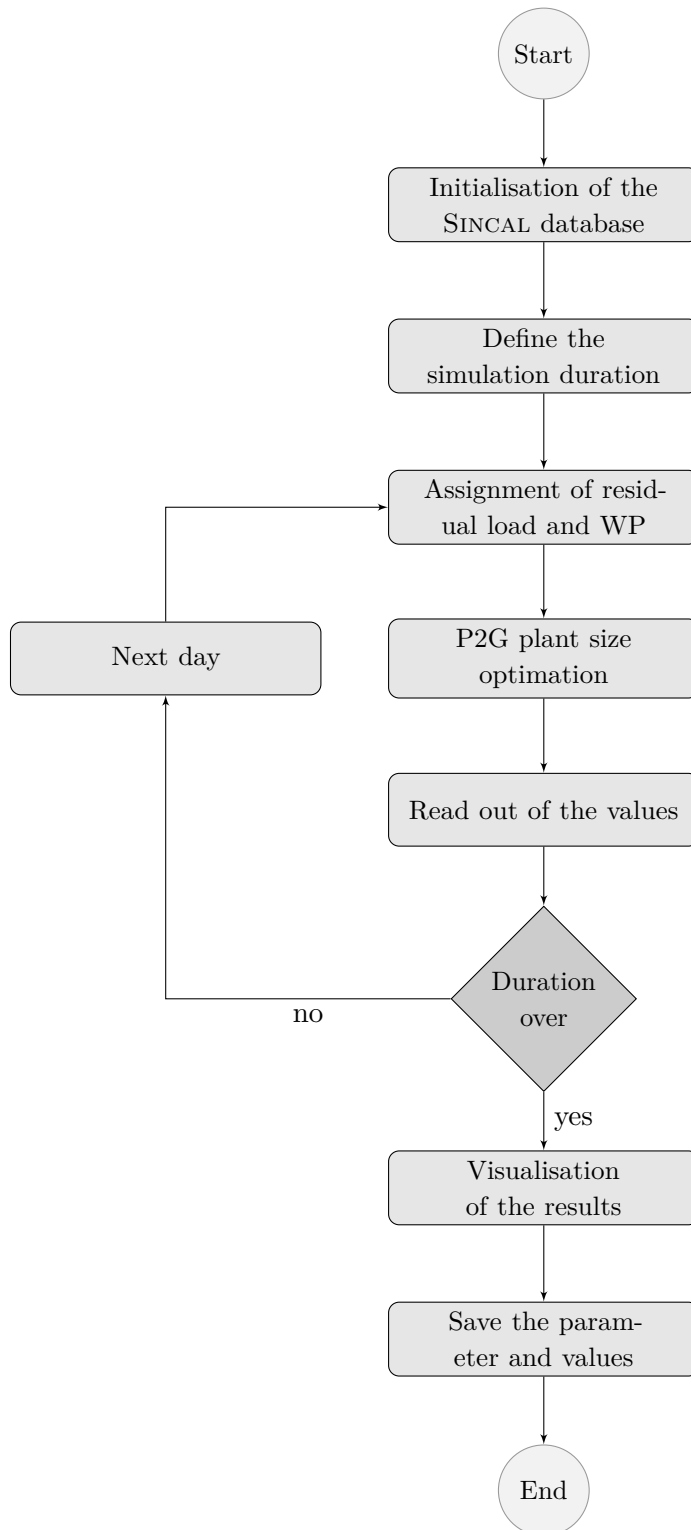
Figure 5.1.: Flow diagram of the Matlab® algorithm

$50\%\hat{P}_{PV,L0} = 26.95\,\text{kWp}$. The load power of private households P_{H0} and agricultures P_{L0} is described in Section 4.2.1.

Simulation is done using two different PV levels. The first level is the maximum possible installable PV power, without upgrading the grids e.g. line expansion and the second PV level is defined to fullfill the energy autarchy of the consumers.

A WP farm in the rural grid is defined as

$$P_{WP} = p_{WP}P_{n,WP} \tag{5.6}$$

with the power profile p_{WP} and the nominal power $P_{n,WP}$ described in Section 4.2.3.

5.1.1. Scenario 1 - Maximum Photovoltaic Power

The maximum PV power, without grid extension is calculated by increasing the PV power and analysing the grid constraints. The limiting grid constraints are the voltage level, line utilisation and transformer utilisation. The most critical parameter, the line utilisation is exceeded before voltage and transformer limitations[6]. The line limitation is given by the utilisation grade I_{line}/I_{th}. The line current I_{line} refers to the thermal current I_{th} and the thermal current is defined by the cable parameters.

In the rural grid the line limitation $I_{line}/I_{th} \le 60\%$ guarantees a N-1 redundancy. According to [1], the N-1 criterion is defined as:

> "The N-1 criterion for system operation is deterministic. It requires that the system be able to tolerate the outage of any one component without disruption and does not concern itself with the probability of an outage. Even if an outage or contingency is highly unlikely, the criterion is still generally applied because system failure when a component is lost is unacceptable."

The maximum PV power of the rural grid with the constraint $I_{line}/I_{th} \le 60\%$ is

$$f_{PV,rural,H0} = f_{PV,rural,L0} = 87\% \tag{5.7}$$

of the installable PV power $\hat{P}_{PV,H0,rural}$ and $\hat{P}_{PV,L0}$.

In the suburban grid for $I_{line}/I_{th} \le 75\%$ the maximum power is $f_{PV,suburban} = 52\%$ of $\hat{P}_{PV,suburban}$. If the P2G plant is placed in the middle of the grid as seen in Figure 4.3, the maximum power can be increased to

$$f_{PV,suburban} = 71\% \tag{5.8}$$

of $\hat{P}_{PV,suburban}$. The P2G plant is placed at the middle node of the grid. Optimal placement reduces power over the lines $L01$-$L05$ by consuming the surplus power, instead of transferring it to transmission grid.

---

[6]A detailed investigation of the grid parameter is done in the master thesis of O. Oberzaucher [38].
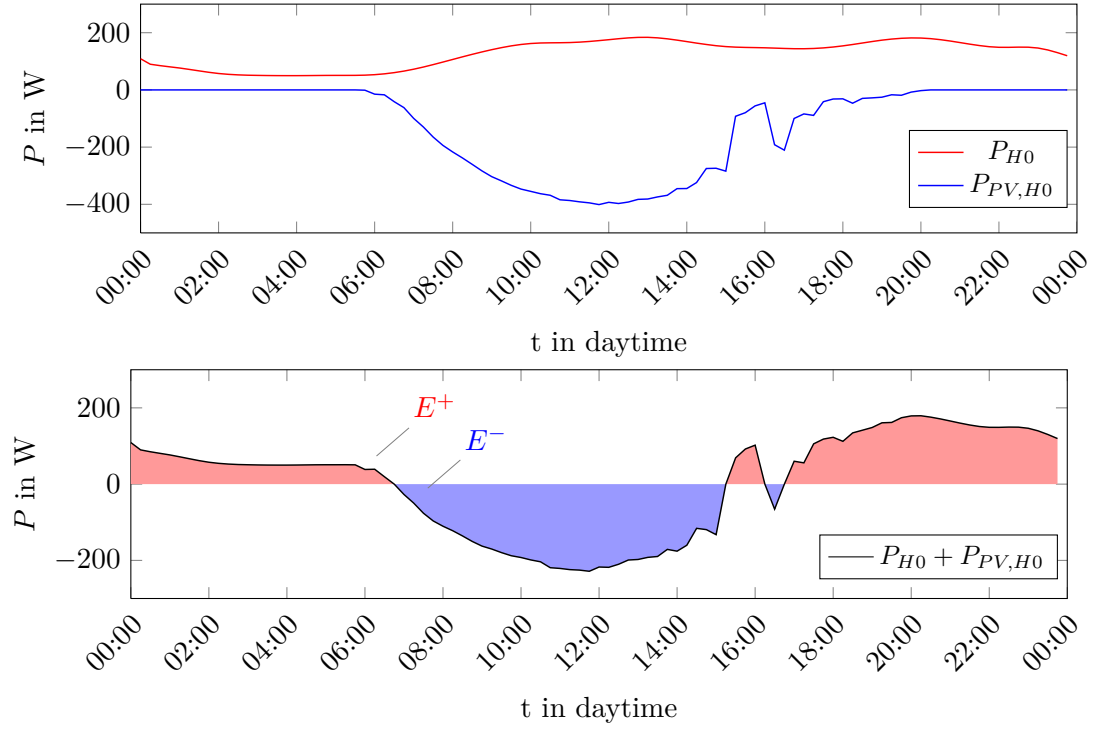
Figure 5.2.: The first plot shows the load power P_{H0} and the PV production $P_{PV,H0}$ of a private household and the second plot shows the residual load $P_{H0} + P_{PV,H0}$ with energies E^+ and E^- calculated by (5.13) and (5.14).

5.1.2. Scenario 2 - **Energy Autarchy**

Energy self-sufficient consumers produce exactly the same energy they are consuming. In case of renewable energy producers, this is only possible with the usage of an energy storage system. The P2G plant enables the transformation of renewable energy into SNG and stores it in the natural gas grid. If the grid's residual load is negative the P2G plant consumes the electrical energy and produces SNG. On the contrary, if the residual load is positive it is possible to convert the SNG back into electrical energy with a Gas Turbine (GT) or a Combined Cycle Gas Turbine (CCGT) power plant. The electricity conversion from SNG to electrical energy is not a part of this work. It is assumed that electrical power produced with GT or CCGT is generated outside the rural and suburban grid. Conversation losses include the transformation from electrical energy to SNG, as well as the reconversion from SNG into electrical energy. The electrical efficiency of a storage cycle

$$\eta_{el} = \eta_{AEL} \, \eta_{meth} \, \eta_{CCGT} = \eta_{P2G} \, \eta_{CCGT} \tag{5.9}$$

consists of the AEL's efficiency, the methanation's efficiency and the efficiency of a CCGT power plant. In this work it is assumed that the electrolyser's efficiency is 75% [46], the

methanation's efficiency 80% [46] and the CCGT efficiency 60% [43]. Total efficiency η_{el} is 36%. In order to calculate the PV power[7] required for a household to be self-sufficient, the residual load over a year

$$P_{sum} = P_{H0} + P_{PV,H0} \tag{5.10}$$

has to be calculated and split into positive residual load power

$$P_{sum}^{+}(t) = \begin{cases} P_{sum,i}(t) & \text{if} \quad P_{sum}(t) > 0 \\ 0 & \text{if} \quad P_{sum}(t) \leq 0 \end{cases} \tag{5.11}$$

and negative residual load power

$$P_{sum}^{-}(t) = \begin{cases} 0 & \text{if} \quad P_{sum}(t) \geq 0 \\ P_{sum,i}(t) & \text{if} \quad P_{sum}(t) < 0 \end{cases} \tag{5.12}$$

and integrated to calculate the positive residual load energy

$$E^{+} = \sum_{i=1}^{365} \int_{0}^{24h} P_{sum}^{+}(\tau)d\tau \tag{5.13}$$

and the negative residual load energy

$$E^{-} = \sum_{i=1}^{365} \int_{0}^{24h} P_{sum}^{-}(\tau)d\tau. \tag{5.14}$$

Figure 5.2 shows this issue in two plots. Negative residual load energy has to be stored and transformed back into electrical energy if the residual load is positive. The storage cycle's efficiency is defined by (5.9). The consumed annual energy has to be equal to the produced annual energy

$$\eta_{el} \, E^{-} \equiv E^{+} \tag{5.15}$$

$$\eta_{el} \sum_{i=1}^{365} \int_{0}^{24h} P_{sum,i}^{-}(\tau)d\tau = \sum_{i=1}^{365} \int_{0}^{24h} P_{sum,i}^{+}(\tau)d\tau. \tag{5.16}$$

The negative energy has to be stored, and therefore it has to be multiplied with the efficiency of the storage cycle. By adopting the peak power of the PV plant using the factor $f_{PV,...}$ energy autarchy is reached. The necessary PV power for a private household in order to achieve energy autarchy

$$\hat{P}_{PV,H0,rural,EA} = \hat{P}_{PV,H0,suburban,EA} = 6.21\,\text{kWp} \tag{5.17}$$

---

[7]The energy produced by the WP plants in the rural grid is not considered.

Table 5.1.: PV power factors for the scenarios: 1) maximum installed PV power to satisfy
the N-1 principle, 2) to guarantee the renewable energy autarchy

Grid Topology	Factor	Maximum	Energy autarchy
rural	$f_{PV,H0,rural}$	87%	45%
	$f_{PV,L0,rural}$	87%	44%
suburban	$f_{PV,suburban}$	71%	71%

and for a agriculture

$$\hat{P}_{PV,L0,EA} = 23.6 \, \text{kWp}. \tag{5.18}$$

The values are

$$f_{PV,rural,H0} = 45.3\%, \; f_{PV,rural,L0} = 43.8\% \; \text{and} \; f_{PV,suburban} = 71.3\% \tag{5.19}$$

of the installable PV power $\hat{P}_{PV,H0,rural}$, $\hat{P}_{PV,L0}$ and $\hat{P}_{PV,H0,suburban}$ presented in beginning of section 5.1.

Table 5.1 lists up the PV power factors for scenario 1 and 2. The suburban's PV power factor of secenario 1 is equal to the PV power factor of scenario 2.

5.2. P2G Optimisation

As mentioned in the beginning of the chapter, the P2G plant represents a variable load in the rural and in the suburban grid. The power of the P2G plant is calculated by an optimisation algorithm implemented in Matlab®. This algorithm optimises the P2G plant's size if a positive surplus power in the grid is available, to minimise the surplus power. If the surplus power is negative the P2G plant is shut down[8].

The optimisation of the P2G plant is done by the combination of a simple interval switching procedure and the method of confidence intervals [30]. Table 5.2 shows the algorithm of this method. To simulate one day Matlab® runs the algorithm 96 times[9]. The function load-flow-calc means the load flow function in PSS®Sincal is operated by Matlab®. A result of the load flow calculation is the power transported over the transformer from or to the high voltage grid. This power P_{ext} is

- **positive** if consumers (agricultures and/or private households) are consuming more electrical power than producing[10] and

---

[8]$P_{P2G} = 0$
[9]$24h/0.25h = 96$
[10]the surplus of energy is negative
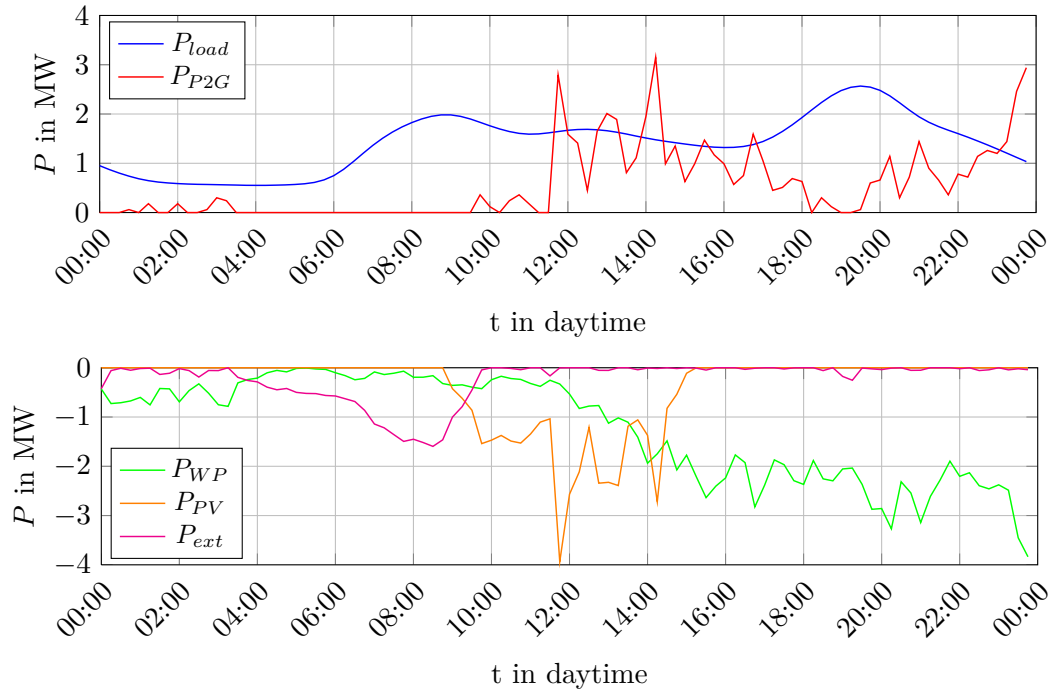
Figure 5.3.: Produced and consumed power in the rural grid, on January 13 2013 for scenario 2. The figure at the top shows the consumed power and the bottom figure the produced power by PV, WP and delivered power from the high voltage grid.

- **negative** if the consumers produce more electrical power as they are consuming[11].

If the power transported over the transformer is negative, power is transmitted from the distribution grid into the transmission grid. In order to avoid feeding back into the higher voltage grid, the P2G plant is installed, to minimise P_{ext}. The power of the P2G plant cannot be negative, because the P2G model of this work is just implemented to transform the electrical energy in one direction, into chemical energy, but not vice versa.

As an example Figure 5.3 shows the produced and consumed energy on January 13 2013, a Sunday in the rural grid in the energy autarchy case. The first plot pictures the consumed power by a load, consisting of private households and agricultures, and the P2G plant. While second plot illustrates the produced energy by PV and WP plants and the delivered power from the high voltage grid. As shown, power from the high voltage grid (P_{ext}) is only negative and therefore used by the distribution grid. If the surplus power is positive [12] the P2G power increases and the surplus power is consumed by the P2G plant.

---

[11] the surplus of energy is positive
[12] the power of the renewable energy sources is bigger than the consumed power

Table 5.2.: P2G optimisation algorithm

Initialisation	$\Delta_0 \in (0, \Delta_{max}]$	(Trust area)
	$P_{P2G,0} \leftarrow P_{prev}$ **or** 0	(P2G start value)
	$P_{ext,0} \leftarrow$ load-flow-calc	(first load flow calculation via PSS®Sincal)
	$k \leftarrow 1$	

repeat

    $\Delta = \Delta_0$

    while $P_{ext} \leq \Delta$ **and** $P_{ext} \geq -\Delta$ **do**

        $\Delta \leftarrow \frac{1}{3}\Delta$

    if $P_{ext,k} < 0$ **do**   feeding back

        $P_{P2G,k} \leftarrow P_{P2G,k-1} + \Delta$ increasing P2G power

        if $P_{P2G,k} < 0$ **do**   only positive P2G power

            $P_{P2G,k} \leftarrow 0$

        else if $P_{P2G,k} < P_{prev}$ **do**   reset

            $P_{P2G,k} \leftarrow P_{prev}$

        end if

    else if $P_{ext,k} > 0$ **do**   feeding

        $P_{P2G,k} \leftarrow P_{P2G,k-1} - \Delta$ decresing P2G power

        if $P_{P2G,k} < 0$ **do**   only positive P2G power

            $P_{P2G,k} \leftarrow 0$

        else if $P_{P2G,k} > P_{prev}$ **do**   reset

            $P_{P2G,k} \leftarrow P_{prev}$

        end if

    end if

    $k \leftarrow k + 1$ next iteration step

    $P_{prev} \leftarrow P_{P2G,k}$

    $P_{ext,k} =$ load-flow-calc   load flow calculation via PSS®Sincal

until $|P_{ext}| < \varepsilon$ **or** $P_{P2G} = 0$

5.3. Analysis

The combined analysis of the P2G plant as a load in the grid is done for two scenarios in the rural and suburban grid.

- **Scenario 1**: The maximum PV power without grid extension is described in Section 5.1.1.

- **Scenario 2**: The installed PV capacity equals energy autarchy mentioned in Section 5.1.2. In this scenario positive surplus energy is transformed to SNG by the P2G plant. The transformation back to electrical energy is not part of this work.

As shown in Table 5.1 scenario 1 equals scenario 2 in the suburban grid. For that reason the investigation of the rural grid is done for scenario 1 and 2, while the investigation in the suburban grid is not differed in scenario 1 or 2. The analysis of maintaining the voltage level, required transformer sizes and choosing different storage locations in rural and suburban grids is described in the master thesis of O. Oberzaucher [38].

5.3.1. One Year Simulation

As written at the beginning of the chapter three months are simulated. In order to extrapolate the period of a year the results of summer and winter months are counted three times each and the results of transitional period six times.

Figure 5.4 and 5.5 show the utilisation curve of the P2G plant of scenario 1 in the rural grid, while Figure 5.6 illustrates the utilisation curve of the P2G plant of the suburban grid. Scenario 2 of the rural grid shows the lower implemented PV power. The utilisation curve of the summer and transitional period are nearly identical, in difference to the winter. The winter curve has only a very short peak, characteristic for less, but strong PV power. By comparing the winter curve of scenario 1 and 2 of the rural grid with the winter curve of the suburban grid the flat part of the power curve in Figure 5.4 is obvious. It is produced by WP and shows the difference between a grid with only PV power and a grid including WP.

The P2G power of a year

$$
\begin{aligned}
P_{P2G}(t) = & \sum_{i=1}^{3} P_{P2G,winter}(i * t_m) + \sum_{i=4}^{6} P_{P2G,TP}(i * t_m) \\
& + \sum_{i=7}^{9} P_{P2G,summer}(i * t_m) + \sum_{i=10}^{12} P_{P2G,TP}(i * t_m), \\
& t \in (0 \dots 360\text{d}), \quad t_m \in (0 \dots 30\text{d})
\end{aligned}
\tag{5.20}
$$

is a result of summing up the months. The yearly utilisation curves of scenarios 1 and 2 in the rural grid are shown in Figures 5.7 - 5.8. The two figures demonstrates the reduced PV power in scenario 2 of the rural grid very well. Figure 5.9 illustrates the

yearly utilisation curve of the suburban grid. In difference to the rural grid, the suburban grid does not include a WP plant and the P2G plant shows a much lower utilisation grade. The maximum P2G power is illustrated in Figure 5.7 and Figure 5.9

$$\hat{P}_{P2G,scx} = \max P_{P2G}, \qquad x \in \{1,2\} \tag{5.21}$$

is used to determine the possible installed capacity of the P2G plant. The possible installed capacity is calculated by reducing the nominal power of the P2G plant

$$P_{n,P2G}(f_{P2G}) = f_{P2G}\hat{P}_{P2G,scx}, \quad f_{P2G} \in \{100\%,\ 75\%,\ 50\%,\ 25\%\}, \quad x \in \{1,2\} \tag{5.22}$$

with the factor f_{P2G}. In this way it is possible to determine the impact of different P2G plants regarding the annual energy. Figures 5.7 - 5.9 show the annual energy converted by a P2G plant

$$E_{P2G,scx}(f_{P2G}) = \int\limits_{0}^{360days} f_{P2G}\ P_{P2G,scx}(\tau)d\tau = \sum_{0}^{360}\int\limits_{i=0}^{24h} f_{P2G}\ P_{P2G,scx}(i*\tau)d\tau \tag{5.23}$$

for the rural and the suburban grid. Four different P2G plant sizes[13] are determined and show very well, that the annual P2G energy is reduced by a smaller P2G plant size.

The power peaks of the PV production are capped by reducing installed capacity of the P2G plant. Figure 5.10 illustrates the power capping on the basis of the first week of April in the suburban grid (scenario 2). The reduction of an annual energy consumption of a P2G plant by reducing the installed capacity is shown in Figure 5.11. The exact values of the annual energy reduction shown in Figure 5.11 are listed in Table 5.3. The reduction of the installed capacity of the P2G plant implemented in the suburban grid effects the converted energy by the P2G plant much more than in the rural grid. The reason is the WP, which is not installed in the suburban grid.

Table 5.3.: Energy $\bar{E}_{P2G,scx}(f_{P2G}) = E_{P2G,scx}(f_{P2G})/E_{P2G,scx}(100\%)$ of the four different P2G plant sizes, illustrated by Figure 5.11.

	$\bar{E}_{P2G,scx}(100\%)$	$\bar{E}_{P2G,scx}(75\%)$	$\bar{E}_{P2G,scx}(50\%)$	$\bar{E}_{P2G,scx}(25\%)$
rural grid, sc.1	100 %	99.4 %	89.3 %	68.1 %
rural grid, sc.2	100 %	99.5 %	93.0 %	70.1 %
suburban grid	100 %	98.0 %	80.8 %	49.5 %

---

[13] $f_{P2G} \in \{100\%,\ 75\%,\ 50\%,\ 25\%\}$
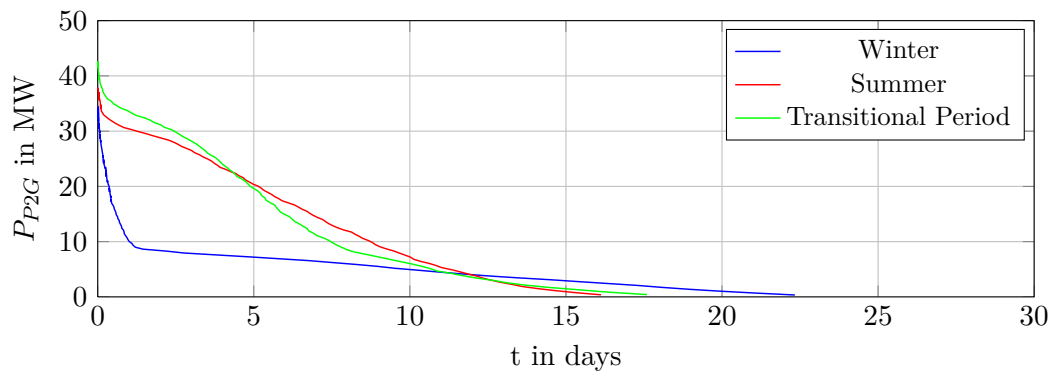
Figure 5.4.: Usage of the P2G plant during a winter, summer and transitional period month in the rural grid of scenario 1
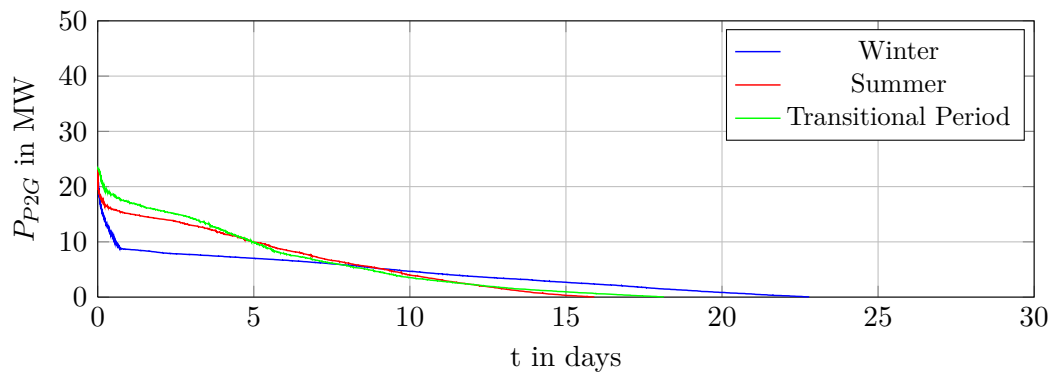
Figure 5.5.: Usage of the P2G plant during a winter, summer and transitional period month in the rural grid of scenario 2
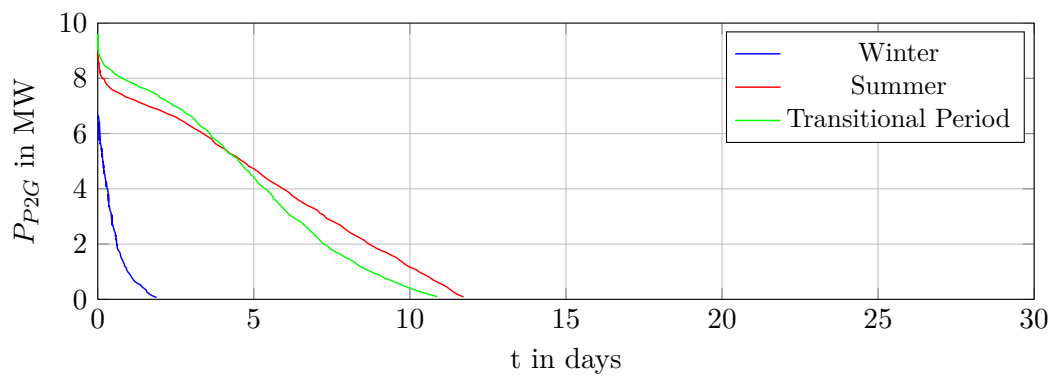
Figure 5.6.: Usage of the P2G plant during a winter, summer and transitional period month in the suburban grid.
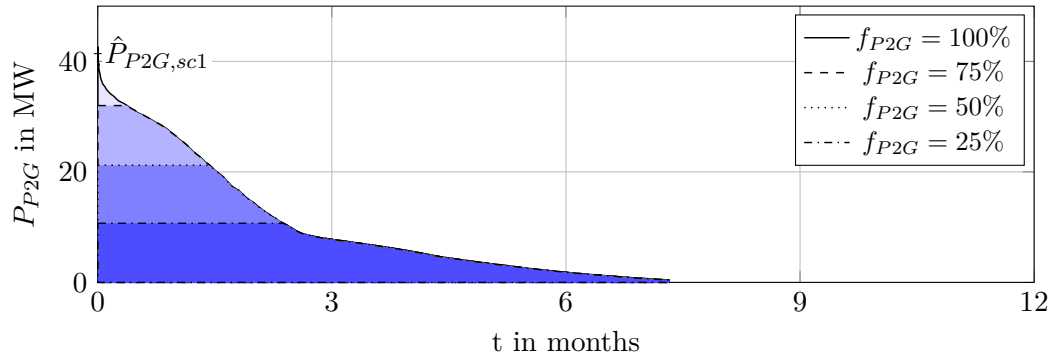
Figure 5.7.: Usage of the P2G plant during a year in the rural grid for scenarios 1 and capping the installed capacity of P2G plant.
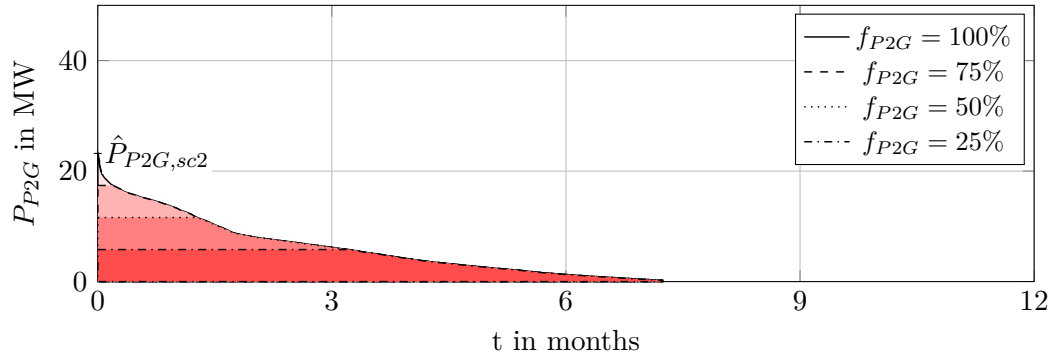
Figure 5.8.: Usage of the P2G plant during a year in the rural grid for scenarios 2 and capping the installed capacity of P2G plant.
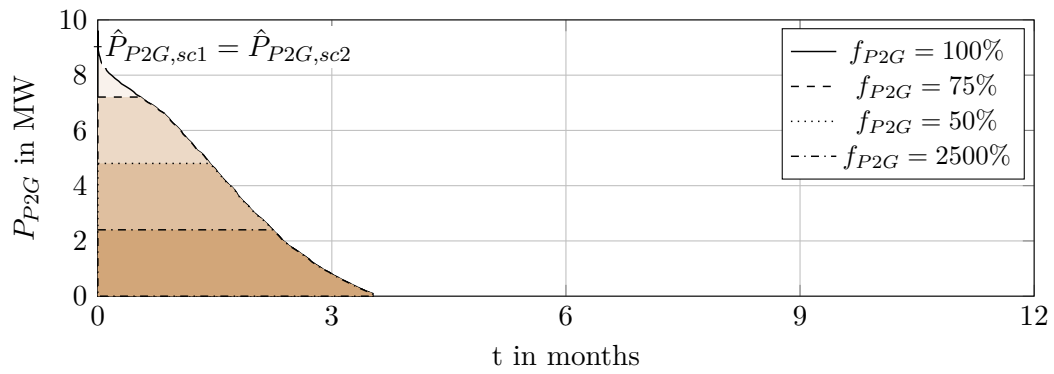
Figure 5.9.: Usage of the P2G plant during a year in the suburban grid for scenario 1 and 2 and capping the installed capacity of P2G plant.
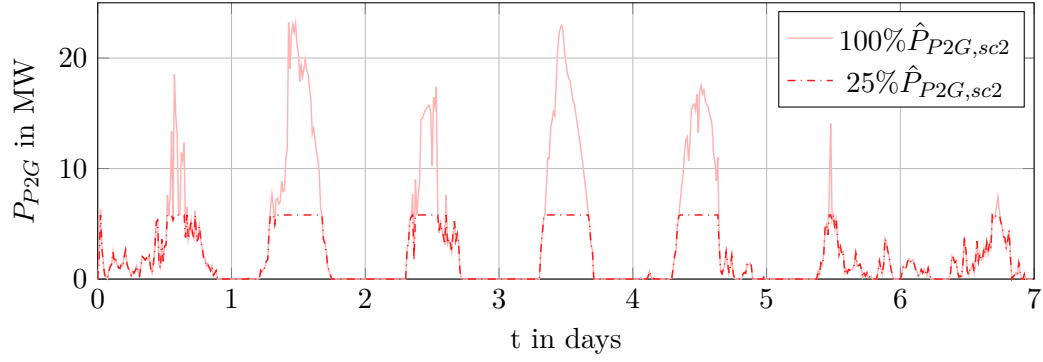
Figure 5.10.: Difference between the power consumption of the $P_{n,P2G} = 100\%\hat{P}_{P2G,sc2}$ and $P_{n,P2G} = 25\%\hat{P}_{P2G,sc2}$ at the first week of April in the suburban grid (scenario 2)
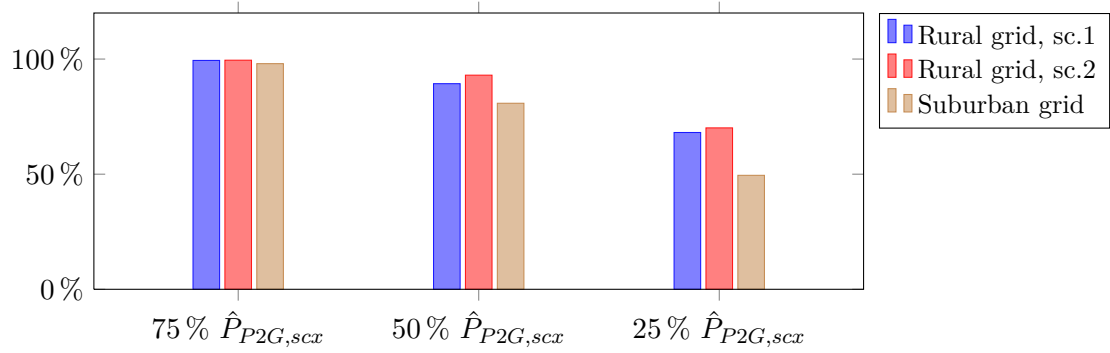
Figure 5.11.: Percentage of energy by a reduced P2G plant size to 75%, 50% and 25% of the maximum appearing P2G energy E_{P2G}.
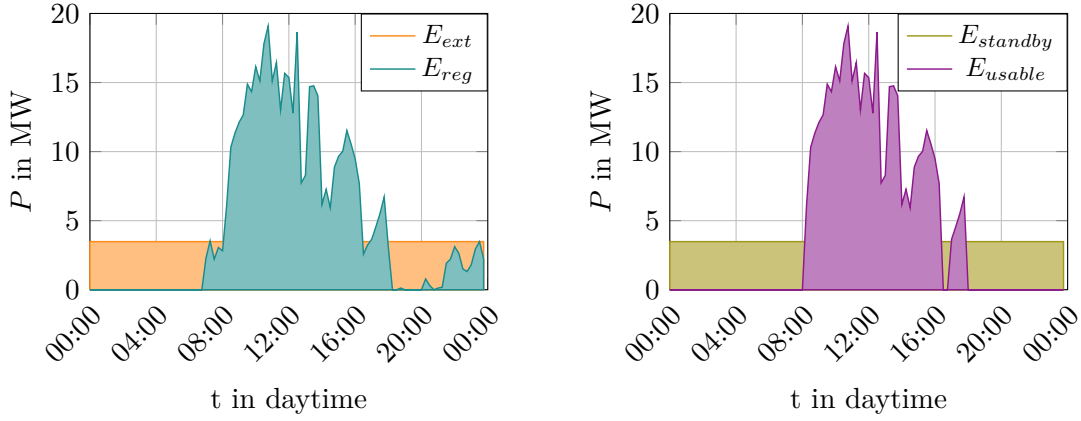
Figure 5.12.: Energies of the electrolyser working in standby mode on April 20 in the rural grid (scenario 2).

5.3.2. The Standby Problem

Under ideal conditions, the P2G plant operates with a constant input power. The P2G plant's input power of this work is produced with renewable energy sources and due to this fact the input power is highly volatile. Most of the today available AEL are able to operate down to $20 - 40\%$ of their nominal power [44]. If the electrolyser's input power is below this value ($20 - 40\%$ of its nominal power), it has to be shut down. In this case the electrolyser is shut down[14], it takes about $30 - 60\,\text{min}$ until the electrolyser is switched on again [50]. The time is needed to purify the AEL with nitrogen [44],[50]. In this time [15] it is not possible to produce hydrogen, if renewable power sources are producing electrical power again.

In this work the minimal necessary AEL input power to avoid AEL's shut down is called standby power. The standby power of an alkaline electrolyser is linear dependent to it's nominal power [24],[37][16]. In this work the assumption of the standby power

$$P_{standby}(f_{P2G}) = 15\% P_{n,AEL}(f_{P2G}) \leq P_{P2G} \tag{5.24}$$

is calculated by the average standby power $10\% P_{n,AEL} \leq P_{standby} \leq 20\% P_{n,AEL}$. It is necessary to keep the AEL at least on standby power, because in that case the electrolyser is able to manage an increasing input power. Another reason for the need of standby is the higher life expectancy of the electrolyser, because a periodical shut-down decreases the electrolyser's performance immensely [7]. The relative high standby power is required

---

[14]According to [24] the electrolyser usually remains well above the standby power and is only shut-down for maintenance.

[15]shut down time + starting time

[16]In comparison to a PEM electrolyser the AEL is only useable above the standby power. PEM electrolysers are workable in $0 \dots 100\%$ of the nominal power [44]

to supply the AEL's auxiliary equipment[17] [11] and ensure a high input dynamic of the AEL. Because the AEL model of Chapter 3 does not include the auxiliary equipment demand the model is expanded. The expansion expresses a H_2 generation stop if the standby power is reached or dropped. For that case the input power is assigned to supply the auxiliary equipment and does not produced H_2.

The standby energy

$$E_{standby, f_{P2G}}(t) = E_{standby}(0) + \int_0^t P_{standby}(\tau, f_{P2G}) d\tau \tag{5.25}$$

results by integrating the AEL's standby power. To conclude only a part of the energy consumed by the electrolyser is used to produce hydrogen. The other part is used to keep the electrolyser at standby mode and supply the auxiliary equipment [50].

Figure 5.12 shows the difference between the energy slices E_{ext}, E_{reg}, $E_{standby}$ and E_{usable} at a typical day. The Energy E_{reg} is the surplus energy produced by regenerative sources (WP and PV) in the grid, but not consumed by the load (private households and/or agricultures), while the E_{ext} represents additional energy

$$E_{ext}(t) = E_{ext}(0) + \int_0^t P_{ext}(\tau) d\tau. \tag{5.26}$$

by integrating the external power

$$P_{ext} = \begin{cases} P_{standby} - P_{reg} & \text{if } P_{reg} < P_{standby} \\ 0 & \text{if } P_{reg} \geq P_{standby} \end{cases} \tag{5.27}$$

needed to keep the P2G plant in the standby mode. E_{ext} is delivered by the high voltage grid and does not necessarily have to be generated by renewable energy sources. The sum of E_{reg} and E_{ext} is the P2G plant's input energy. The energy balance

$$E_{ext} + E_{reg} \equiv E_{standby} + E_{usable} = E_{P2G} \tag{5.28}$$

of Figure 5.12 must be satisfied.

As mentioned at the beginning of this section only a part of the input power is used to produce hydrogen. The remaining power supplies the auxiliary equipment. Due to this fact the energies of Figure 5.12 are indicated otherwise. E_{usable} marks the H_2 producing energy and $E_{standby}$ the non-H_2 producing energy. $E_{standby}$ represents the energy used to supply the auxiliary equipments, while E_{usable} produces H_2 with the AEL's efficiency η_{AEL}[18]. The further transformation to SNG includes the efficiency η_{meth} and an entirely P2G plant efficiency $\eta_{P2G} = \eta_{AEL}\eta_{meth}$.

---

[17]such as heaters, heat exchangers, gas driers, pumps and deoxidisers.

[18]η_{AEL} includes the conversation losses due to the operation of auxiliary devices and generation of heat.

Table 5.4.: $E_{usable}(1\,a, f_{P2G})$ and P2G plant's full load hours of (5.30) of the two scenarios and the different P2G plant sizes including the standby mode.

f_{P2G}	100%	75%	50%	25%
rural grid, sc.1	48.10 GWh $\widehat{=}1125\,h$	49.96 GWh $\widehat{=}1561\,h$	44.98 GWh $\widehat{=}2108\,h$	32.30 GWh $\widehat{=}3030\,h$
rural grid, sc.2	23.20 GWh $\widehat{=}1236\,h$	17.40 GWh $\widehat{=}1712\,h$	11.60 GWh $\widehat{=}2388\,h$	5.80 GWh $\widehat{=}3483\,h$
suburban grid	9.64 GWh $\widehat{=}1003\,h$	9.55 GWh $\widehat{=}1325\,h$	7.9 GWh $\widehat{=}1644\,h$	4.83 GWh $\widehat{=}2012\,h$

The Figures 5.14-5.16 illustrate the yearly results[19] of

$$E(t, f_{P2G}) = E(0) + \int_0^t E(\tau, f_{P2G}) d\tau, \quad E \in \{E_{reg}, E_{ext}, E_{usable}, E_{standby}\}. \qquad (5.29)$$

As mentioned at the beginning of this chapter, the annual results are the extrapolation of counting the results of summer and winter month three times each and the results of transitional periods six times. Table 5.4 shows the exact values of $E_{useable}$ and the resulting full load hours

$$t_{FL}(f_{P2G}) = \frac{E_{usable}(1\,a, f_{P2G})}{f_{P2G}\hat{P}_{P2G}} = \frac{E_{useable}(1\,a, f_{P2G})}{P_{n,P2G}(f_{P2G})}, \qquad (5.30)$$
$$f_{P2G} \in \{100\%, 75\%, 50\%, 25\%\}.$$

The full load hours are calculated with E_{usable}, because only E_{usable} is the energy slice responsible for the H_2 (and SNG) -production. As shown in Table 5.4 full load hours increase significantly at smaller installed P2G capacity. The scenarios in the rural grid present much higher full load hours as those in the suburban grid. Reasonable for this is the missing WP in the suburban grid.

Table 5.4 and Figures 5.14-5.16 demonstrate very well that a greater installed (greater f_{P2G}) P2G capacity does not imply a bigger production of H_2 (and SNG). E_{usable} at $f_{P2G} = 75\%$ and $f_{P2G} = 50\%$ in the rural grid is even bigger than the usable energy at $f_{P2G} = 100\%$. The reason for this is that a smaller nominal capacity of the P2G plant implies a smaller standby power. Another reason is that a P2G plant with a smaller nominal capacity works with that input power and produces H_2 (and SNG), which is smaller than the standby power of a P2G plant with greater capacity. That means a P2G plant with great capacity often does not even produce H_2 (and SNG) when the same input power of a P2G plant with a small capacity is already greater than it's standby power.

---

[19]$t = 1\,a = 365\,d$

By comparing the results of the rural grid to those of the suburban grid it is obvious that the ratio of $E_{usable}/E_{standby}$, in the suburban grid is much higher than this ratio in rural grid. It is caused by the missing WP plant in the suburban grid. WP is often produced during night hours or during winter months and it represents an optimum counterpart to PV power production.

A possibility to reduce standby losses, is to ensure a minimal operating mode of the AEL. That means that the AEL has at least to work at the lower partial load range of

$$P_{partial}(f_{P2G}) = 30\% P_{n,AEL}(f_{P2G}) \leq P_{P2G}. \tag{5.31}$$

Figure 5.13 shows the changed energy slices in comparison to Figure 5.12. The advantage of this method is that $E_{standby}$ is not used to supply the AEL's auxiliary equipment. By increasing E_{usable} the amount of produces H_2 (and SNG) increases as well. Disadvantageous is the enhanced need of external power and for that reason external energy E_{ext}. The usable energy E_{usable} results in

$$E_{useable} = E_{ext} + E_{reg} = E_{P2G} \tag{5.32}$$

and raises significantly. E_{usable} is transformed in H_2 with the AEL's efficiency η_{AEL}.
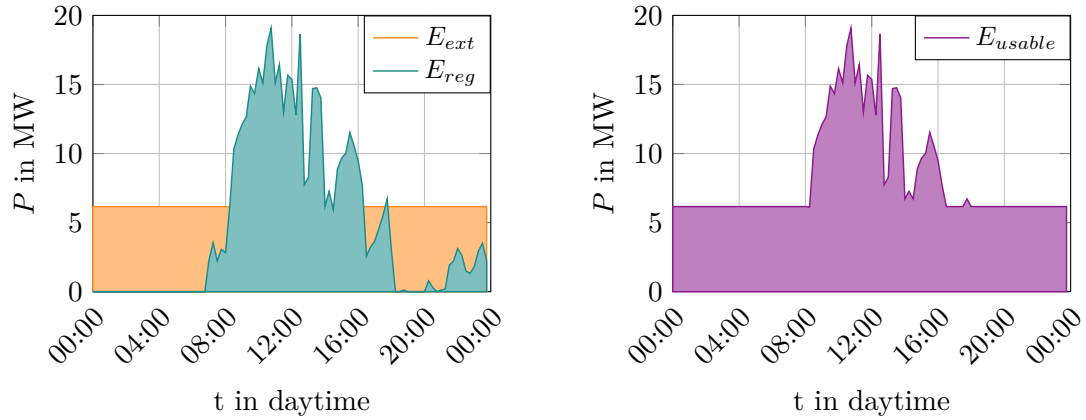
Figure 5.13.: Energies of the electrolyser working in minimal operating mode on April 20 in the rural grid (scenario 2).
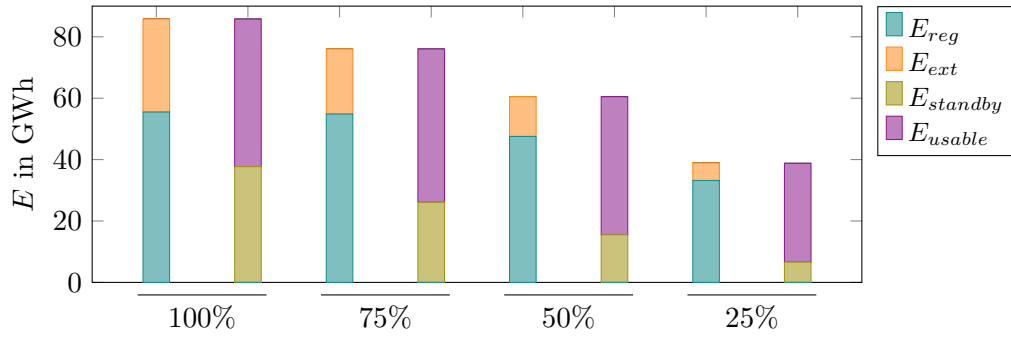
Figure 5.14.: Energy results in the rural grid scenario 1, based on four different P2G plant sizes including standby mode demand.
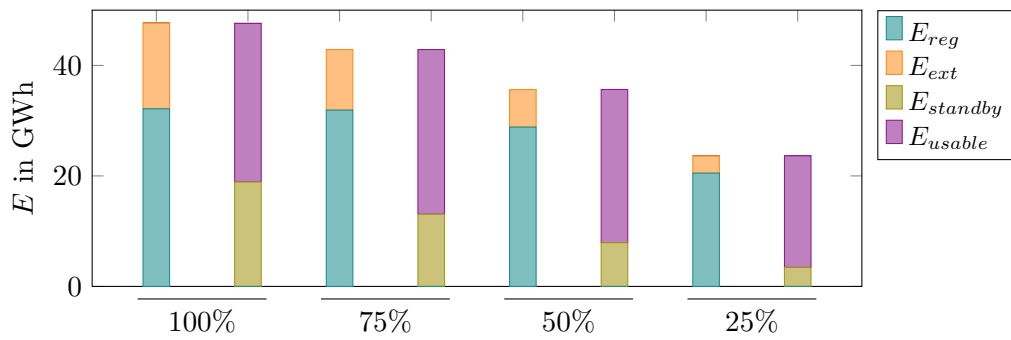
Figure 5.15.: Energy results in the rural grid scenario 2, based on four different P2G plant sizes including standby mode demand.
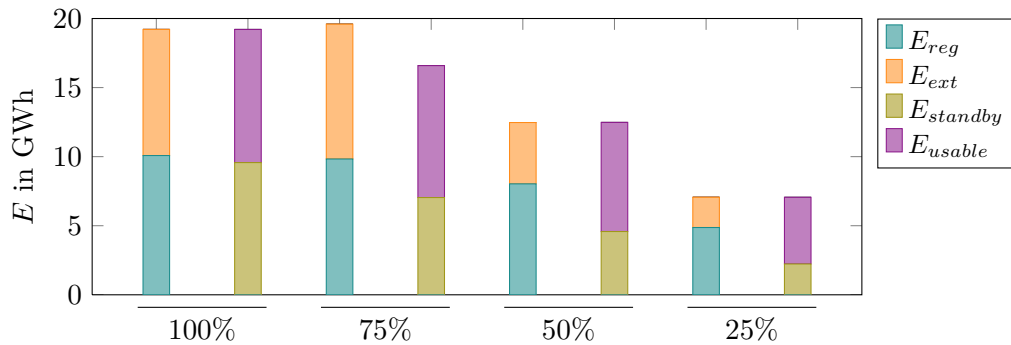
Figure 5.16.: Energy results in the suburban grid, based on four different P2G plant sizes including standby mode demand.
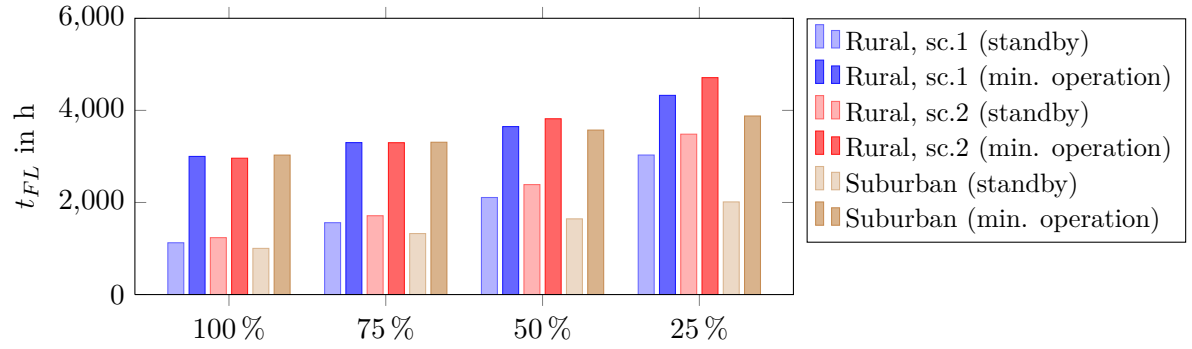
Figure 5.17.: Full load hours of the two scenarios at $f_{P2G} \in \{100\%, 75\%, 50\%25\%\}$ of the maximum appearing P2G power $\hat{P}_{P2G}$ with the standby and minimal operating mode.

Figures 5.18-5.20 show the higher E_{use} and E_{ext} by comparing them to Figures 5.14-5.16. In some cases the external energy E_{ext} is even bigger as the energy E_{reg} produced by renewable energy sources. For that the reason the demand on external energy increases dramatically by operating the P2G plant in the minimal operating mode. The downside of the minimal operating mode is the higher external power consumption. By investigating the suburban grid it shows very well that a grid without WP needs a much higher external energy demand. The full load hours (5.30) are much higher with a higher E_{usable}, as shown in Figure 5.17.
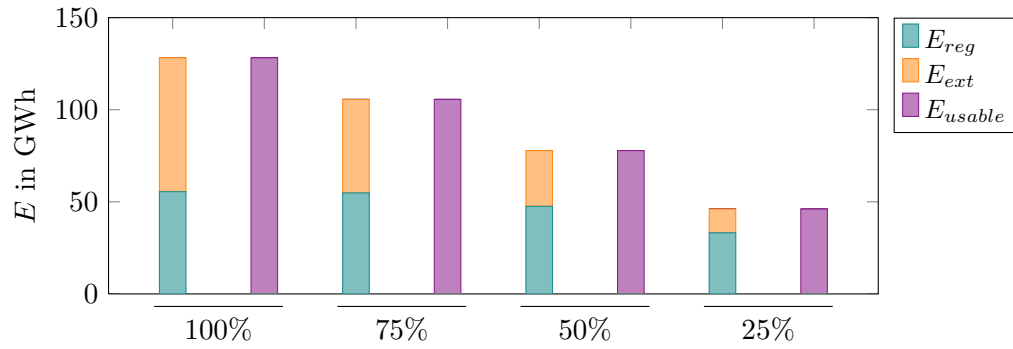
Figure 5.18.: Energy results in the rural grid scenario 1, based on four different P2G plant sizes including minimal operating mode demand.
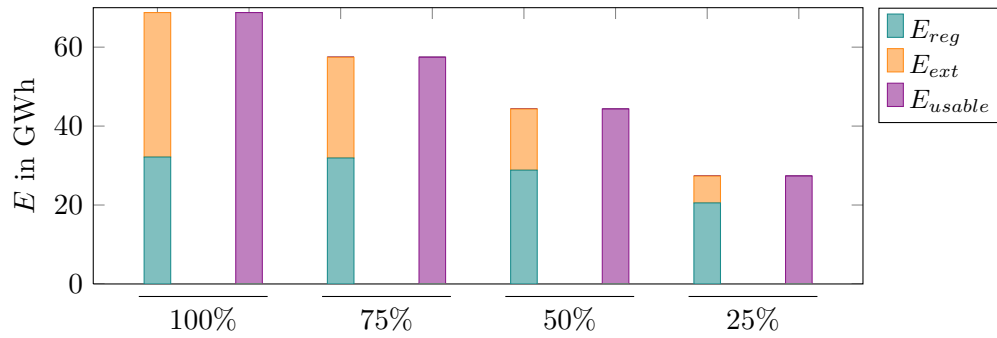
Figure 5.19.: Energy results in the rural grid scenario 2, based on four different P2G plant sizes including minimal operating mode demand.
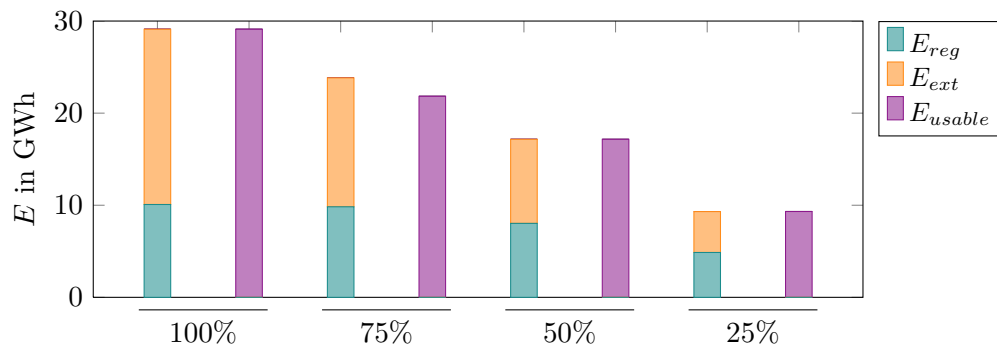
Figure 5.20.: Energy results in the suburban grid, based on four different P2G plant sizes including minimal operating mode demand.
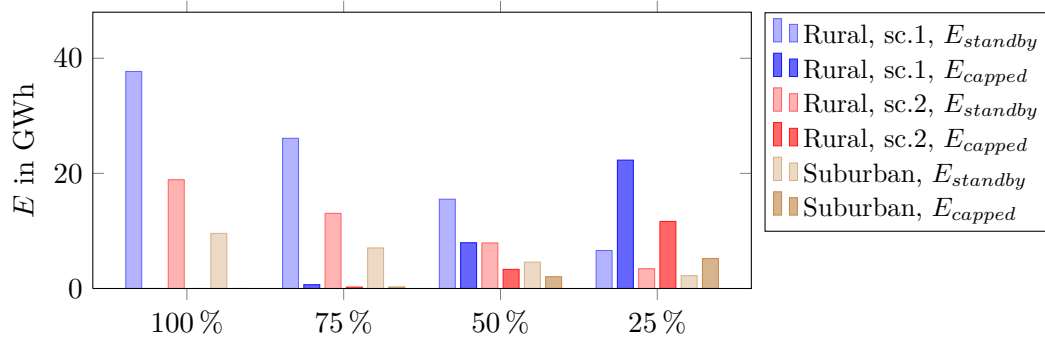
Figure 5.21.: Standby energy $E_{standby}$ and the capped regenerative surplus energy E_{capped} at $f_{P2G} \in \{100\%, 75\%, 50\% 25\%\}$.

5.3.3. Standby Battery

The idea of a standby battery is to reduce the power consumption of the high voltage grid for the standby mode of a P2G plant, by installing a second storage system. It can be done by storing the power peaks in batteries, instead of capping the power generation, as it is presented in 5.3.1. The capped regenerative energy

$$E_{capped}(t, f_{P2G}) = E_{reg}(t, 100\%) - E_{reg}(t, f_{P2G}), \quad f_{P2G} = \{75\%, 50\%, 25\%\} \quad (5.33)$$

increases by a smaller installed P2G capacity. For that reason (with a battery) storable energy increases to a maximum with $f_{P2G} = 25\%$. Figure 5.21 illustrates that the capped renewable energy for the rural and the suburban grid at $f_{P2G} = 25\%$ is even bigger than the required standby energy. If $f_{P2G} = 100\%$ the installation of a battery system is useless because $E_{capped} = 0$. The required battery size can be calculated as

$$E_{batt}(t, f_{P2G}) = \frac{E_{ext}(t, f_{P2G})}{t} = \frac{E_{ext}(1\,\mathrm{a}, f_{P2G})}{1\,\mathrm{a}}, \quad f_{P2G} \in \{100\%, 75\%, 50\%, 25\%\}.$$
$$(5.34)$$

This energy E_{batt} is an estimation of the minimum battery capacity required to reduce the external power consumption of a P2G plant for standby mode. For example during a cloudy windless week, the battery capacity E_{batt} is too small to guarantee the standby power of the P2G plant. Figure 5.22 illustrates the minimum battery capacity depending on the P2G plant's nominal capacity.

The linear relation of E_{batt} to $P_{n,P2G}$ can be approximated by

$$E_{batt}(P_{n,P2G}) = e_0 + e_1 P_{n,P2G}. \quad (5.35)$$

According to Figure 5.22 the straight line of scenario 1 in the suburban grid has the same trend as the line of scenario 2 in the suburban grid. For that reason the approximation is done for a battery in a grid with WP and PV (approximation 1) and in a grid with only

PV (approximation 2). It is obvious that the battery capacity in a grid with only PV has to be greater than the battery capacity in a grid with WP and PV. The two different approximations are shown in Figure 5.22 too. The numerical parameters of (5.35) are listed in Table A.17.
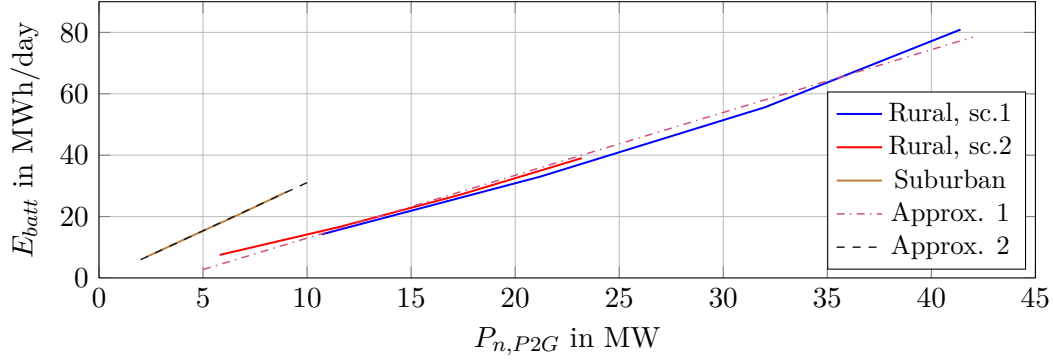
Figure 5.22.: Minimum battery capacity in dependence of the P2G plant's nominal power and the approximations according to (5.35) of the rural grid (approximation 1) and the suburban grid (approximation 2).

5.3.4. Efficiency

The overall efficiency of the P2G plant

$$\eta_{P2G}(t, f_{P2G}) = \eta_{AEL}(t, f_{P2G})\ \eta_{meth}(t, f_{P2G}) \tag{5.36}$$

consists of the AEL's efficiency and the methanation's efficiency. The AEL's efficiency is not constant over the full input power range. Section 3.1.3 and especially Figure 3.8 describe the AEL's power dependency. According to Chapter 3 the alkaline electrolyser's efficiency is inversely proportional to the input power. That means the AEL's efficiency is larger in the partial load, than under full load. The AEL's efficiency

$$
\eta_{AEL}(t, f_{P2G}) = \frac{E_{H_2}(t, f_{P2G})}{E_{P2G}(t, f_{P2G})} = \frac{LHV_{H_2}\left(V_{H_2,0} + \int\limits_0^t \dot{V}_{H_2}(\tau, f_{P2G})d\tau\right)}{E_{P2G,0} + \int\limits_0^t P_{P2G}(\tau, f_{P2G})d\tau}
$$
$$
= \frac{LHV_{H_2}\ V_{H_2}(t, f_{P2G})}{E_{P2G,0} + \int\limits_0^t P_{P2G}(\tau, f_{P2G})d\tau} \tag{5.37}
$$

equals produced H_2's energy content divided by the electrical input energy . E_{H_2} is calculated with the lower heating value $LHV_{H_2} = 3\,\text{kWh/Nm}^3$ [44] and the produced volume of hydrogen V_{H_2} with the start volume $V_{H_2,0}$ at $t = 0$. While E_{usable} represents

the integral of electrical input power with the start value $E_{usable,0}$ at $t = 0$.

The methanation's efficiency

$$\eta_{meth}(t, f_{P2G}) = \frac{E_{CH_4}(t, f_{P2G})}{E_{H_2}(t, f_{P2G})} = \frac{HHV_{CH_4}\left(V_{CH_4,0} + \int\limits_0^t \dot{V}_{CH_4}(\tau, f_{P2G})d\tau\right)}{LHV_{H_2}\left(V_{H_2,0} + \int\limits_0^t \dot{V}_{H_2}(\tau, f_{P2G})d\tau\right)}$$

$$= \frac{HHV_{CH_4}V_{CH_4}(t, f_{P2G})}{LHV_{H_2}V_{H_2}(t, f_{P2G})} \tag{5.38}$$

is calculated by dividing the energy content of produced SNG by the energy content of produced H_2. While the energy content of H_2 is determined with the lower heat value LHV_{H_2} the SNG's energy content results in the product of SNG volume with the higher heat value $HHV_{CH_4} = 11.06\,\text{kWh/Nm}^3$ [44].

Figures 5.23 and 5.24 show the yearly production of synthetic methane [20] for the maximum ($f_{P2G} = 100\%$) and minimum ($f_{P2G} = 25\%$) P2G plant size. The left picture shows the yearly SNG production by standby mode in the operation strategy of P2G plant in the left picture and the minimal operating mode in the right picture.

A year is divided into

- month 1 to 3 as winter,

- month 4 to 6 as transitional period,

- month 7 to 9 as summer and

- month 10 to 12 as transitional period months.

During the winter months in the standby mode the SNG production is very low or nearly zero in the suburban grid because of $\dot{V}_{H_2} = 0$ and $\dot{V}_{CH_4} = 0$ for $P_{P2G} = P_{standby}$. During the summer and transitional period the gradient of SNG production is almost constant. The CH_4 production in the minimal operating mode is quite constant over a year. It is because of $P_{partial} > P_{standby}$ and with $\dot{V}_{H_2} > 0$ and $\dot{V}_{CH_4} > 0$ for $P_{P2G} = P_{partial}$ methane is even produced during times the P2G plant is in the partial mode.

Figure 5.25 and Table 5.5 show the average efficiency of the P2G plant. The higher efficiency of a P2G plant in the minimal operating mode is obvious. Although the efficiency of the P2G plant is almost constant in the minimal operating mode, smaller plant sizes are lowering it. The reason is higher full load hours (Figure 5.17) of smaller

---

[20] $t = 360$days for (5.36)-(5.38)

Table 5.5.: η_{P2G} of two scenarios and the different P2G plant sizes in standby mode and minimal operating mode.

f_{P2G}		100%	75%	50%	25%
rural grid, scenario 1	standby mode	33.89 %	38.9 %	43.5 %	48.07 %
	minimal operating mode	61.05 %	60.4 %	59.8 %	59.03 %
rural grid, scenario 2	standby mode	36.20 %	41.15 %	45.37 %	49.02 %
	minimal operating mode	61.21 %	60.56 %	59.75 %	58.64 %
suburban grid	standby mode	30.34 %	33.79 %	36.44 %	39.04 %
	minimal operating mode	60.91 %	60.32 %	59.87 %	59.43 %

P2G plants. The efficiency of the P2G plant in the standby mode is increasing with the reduction of installed P2G capacity . This behaviour is explainable with

$$\frac{E_{useable}(t, 100\%)}{P_{n,P2G}(100\%)} < \frac{E_{useable}(t, 75\%)}{P_{n,P2G}(75\%)} < \frac{E_{useable}(t, 50\%)}{P_{n,P2G}(50\%)} < \frac{E_{useable}(t, 25\%)}{P_{n,P2G}(25\%)} \ . \qquad (5.39)$$

It means the proportion of usable energy to nominal power of a bigger plant is lower to the proportion of a smaller plant .
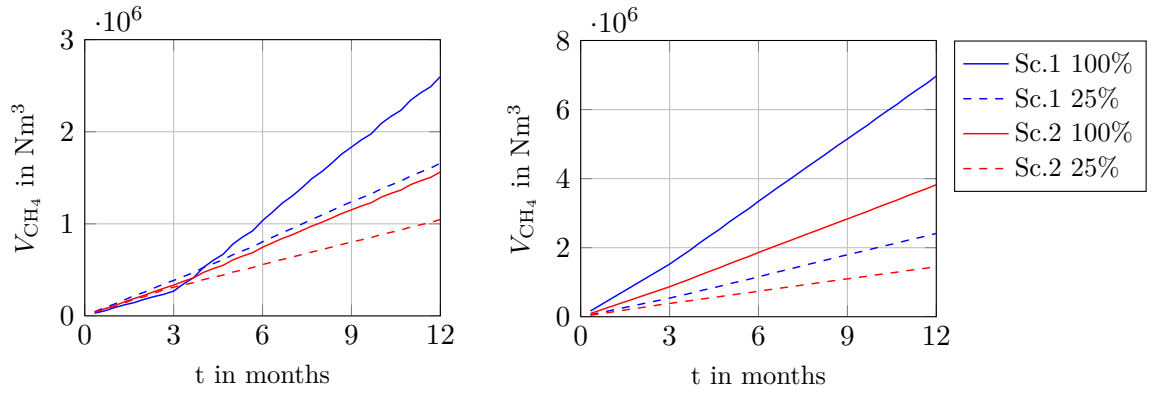
Figure 5.23.: Yearly produced V_{CH_4} in the rural grid for scenarios 1 and 2, in standby mode (left figure) and minimal operating mode (right figure).
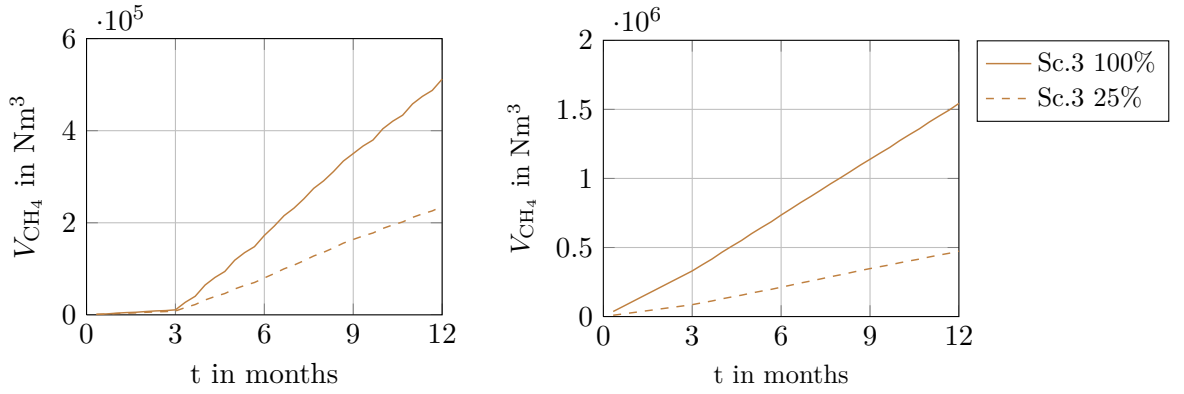
Figure 5.24.: Yearly produced V_{CH_4} in the suburban grid, in standby mode (left figure) and minimal operating mode (right figure).
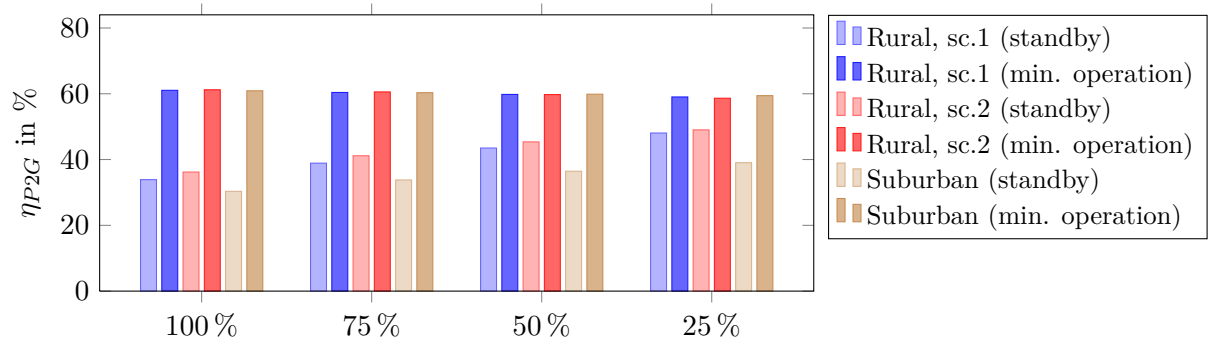
Figure 5.25.: P2G efficiency $\eta_{P2G}(1\,a, f_{P2G})$ of the rural and suburban grid with $f_{P2G} \in \{100\%, 75\%, 50\%, 25\%\}$ at standby and minimal operating mode.
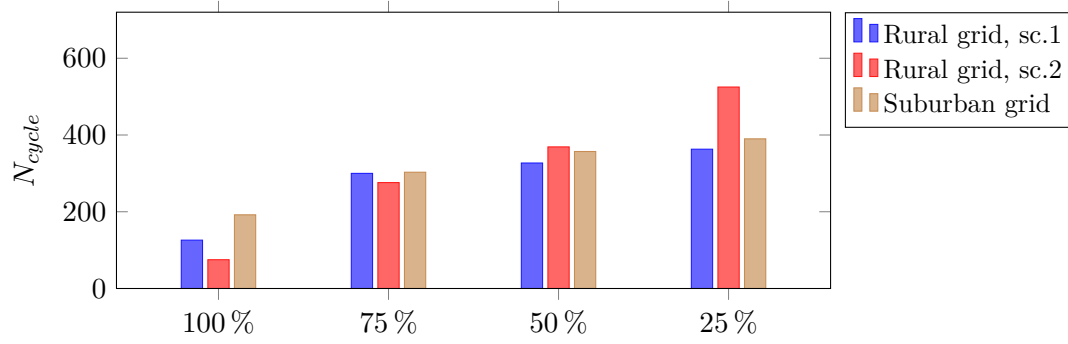
Figure 5.26.: Cycles during a year in the rural and the suburban grid at $f_{P2G} \in \{100\%, 75\%, 50\%25\%\}$.

5.3.5. Cycle Number

The dynamic and volatility of the P2G plant's input power determines the cycles of a P2G plant. A cycle is similar to the charge cycle of a battery. In this work one cycle of a P2G plant is defined by raising the input power from

$$P_{cycle,min} = 30\%P_{n,P2G} \tag{5.40}$$

up to

$$P_{cycle,max} = 80\%P_{n,P2G}. \tag{5.41}$$

By decreasing the power down to $P_{cycle,min}$ one cycle is finished[21]. The amount of cycles is mode-independent, i.e. they stay constant if the P2G plant works in the standby mode or in minimal operating mode. Due to $P \leq P_{cycle,min}$ with $P \in \{P_{standby}, P_{partial}\}$ and therefore the lower bound is not exceeded variously.

Figure 5.26 shows the amount of cycles in both modes. The increasing number of cycles by decreasing f_{P2G} is well recognisable. For that reason the partial derivative of the number of cycles

$$\frac{\partial N_{cylce}}{\partial f_{P2G}} < 0 \tag{5.42}$$

in respect to f_{P2G} is negative. This occurrence is explainable by the effect of reducing the P2G plant's installed capacity which causes a match of the capped regenerative power peaks with one hysteresis cycle. Especially in the rural grid at scenario 2 and $f_{P2G} = 25\%$ the cycle number is very high because in this scenario the WP is almost as powerful as the PV.

The cycles are directly proportional to the life expectancy of a P2G plant. Unfortunately until now no scientific work discussing this relationship is published.

---

[21]comparable to one hysteresis cycle

6. Summary and Outlook

Chapter 3 of this work shows a complete scalable mathematical model of a P2G plant. The high detailed P2G model consists of an AEL and a methanation. The input characteristics of the electrolyser and therefore the P2G plant show that it is possible to follow each power gradient[1]. The requirement for the AEL's permanent dynamic is the constraint $P_{P2G} \geq P_{standby}$. If this requirement is fulfilled the electrolyser stays at operating temperature and is capable for a dynamic loading. Due to the fact that the time sample of the combined simulation is 15 min, the P2G plant's dynamic can be considered as sufficient.

Two model regions, a representative rural and suburban grid, are introduced for the combined simulation of the P2G plant which is explained in Chapter 4. Another part of this Chapter is the definition and explanation of the load of private households and agricultures, PV and WP profiles are used in this work. The optimal position of the P2G plant in the rural grid is the node next to the transformer, while the optimal position in the suburban grid is the grid's middle node.

The combined simulation of the P2G plant model and the electrical grids is subject of Chapter 5. The beginning of the chapter introduces the program's algorithm, controlled by MATLAB® and simulated in PSS®SINCAL. An optimisation algorithm modifies the P2G plant size considering the relation to surplus power. The optimisation algorithm consists of the combination of a simple interval switching procedure and the method of confidence intervals.

As written at the beginning of Chapter 5 three months are simulated. In order to extrapolate the period of a year, the results of summer and winter months are counted three times each and the results of transitional period six times. Two scenarios with different PV power levels are developed for combined simulation. Scenario 1 identifies the maximum PV power due to limiting grid constraints, while scenario 2 calculates the PV power necessary for an energy autarchy operation of the grid[2].

The result of the annual simulation shows that a reduction of the P2G plant size increases the annual full load hours dramatically. The main problem of an AEL is the minimal required standby power of $P_{P2G,min} = 15\% P_{n,P2G}$. The demand on standby

---

[1]For example the electrolyser NEL P-60 offers a ramp-up time to maximum capacity from stand-by of $< 6\,\mathrm{s}$[37].

[2]As mentioned in 5.1.2 the model of a GT or a CCGT to transform the SNG back to electrical energy is not a part of this work.

power stays constant. For that reason the P2G plant has to be supplied with external electricity at times of low renewable power production as well. Due to this fact, it is not possible to guarantee a purely regenerative operation of the P2G plant[3].

If the AEL operates at standby power, the produced H_2 can not further be used, because of the low product gas quality[4]. By operating the P2G plant in the minimum operation mode of $P_{P2G,min} = 30\% P_{n,P2G}$ it is possible to use the produced hydrogen. For that reason the efficiency of the P2G plant raises significantly by working in minimum operating mode instead of standby power. The problem of minimum operating mode is the increasing external power consumption of the grid, i.e. the external power is not necessarily renewable energy [5].

The introduction of a standby battery enables the storage of capped renewable energy. The storage of energy is only possible if the nominal power of a P2G plant is smaller than the peak power of the surplus energy. The battery appropriates the coverage of the standby power demand, by decreasing external energy demand. By counting the on-off cycles of the electrolyser, it is illustrated that higher full load hours are accompanied with increasing number of cycles[6].

To optimise storage of electrical energy by a P2G plant, it is recommended

- to operate the P2G together with WP and PV. The nominal power to this two power plants should be similar, to support each other e.g. sunny windless days or cloudy high wind days.

- If only PV is available the P2G plant has to shut down in winter months to avoid the standby problem[7].

- A small P2G plant guarantees high full load hours by a low standby energy.

- A battery (or another optional storage system) is installed to use the surplus power peaks and reduce the external power consumption.

- To increase yearly efficiency the P2G plant is operated above standby power (minimum operating mode).

---

[3]If the external power originates from hydro power plants, or other WP plants a purely renewable operation is possible.

[4]The amount of O_2 in the H_2 flow is too high.

[5]generated through PV, wind, water or biomass

[6]Only valid in this work, because the input power of the P2G plant is very dynamic, due to the high volatility of regenerative power sources.

[7]The restart of a turned off AEL/P2G is very energy-intensive [44]. For that reason AEL are rarely shut down [24].

A. Numerical Values

This chapter includes the numerical parameter values of this work.

A.1. Electrochemical Model

Table A.1.: Parameters of cell voltage (3.26) according to [49]

r_1	r_2	s
$8.05 \times 10^{-5}\,\Omega\text{m}^2$	$-2.5 \times 10^{-7}\,\text{ohm m}^2\,/°\text{C}$	$0.185\,\text{V}$

t_1	t_2	t_3
$-1.002\,\text{m}^2/\text{A}$	$8.424\,\text{m}^2°\text{C}/\text{A}$	$247.3\,\text{m}^2°\text{C}^2/\text{A}$

Table A.2.: Numerical values of the temperature dependent term (3.34) in (3.33) according to [10]

u_1	u_2	u_3	u_4
$1.5184\,\text{V}$	$1.5421 \times 10^{-3}\,\text{V}/°\text{C}$	$9.526 \times 10^{-5}\,\text{V}/°\text{C}$	$9.84 \times 10^{-8}\,\text{V}/°\text{C}^2$

Table A.3.: Numerical values of (3.36) in (3.35) according to [10]

$a_{1,1}$	$a_{1,2}$	$a_{1,3}$
$-0.0348\,\text{kg mol}^{-1}$	$-3.8646 \times 10^{-3}\,\text{kg}^2/\text{mol}^2$	$5.1998 \times 10^{-5}\,\text{kg}^3/\text{mol}^3$

Table A.4.: Numerical values of (3.37) in (3.35) according to [10]

$a_{2,0}$	$a_{2,1}$	$a_{2,2}$	$a_{2,3}$
1	$-1.2062 \times 10^{-3}\,\text{kg mol}^{-1}$	$5.6024 \times 10^{-4}\,\text{kg}^2/\text{mol}^2$	$7.8228 \times 10^{-6}\,\text{kg}^3/\text{mol}^3$

Table A.5.: Numerical values of the constants in (3.38) for the vapour pressure of pure water according to [10]

b_1	b_2	b_3	b_4
81.6179	$-7.699 \times 10^3\,°\text{C}$	10.9	$9.5891 \times 10^{-3}\,°\text{C}^{-1}$

Table A.6.: Numerical values of the constants in (3.39) for the water activity according to [10]

c_1	c_2	c_3	c_4
$-0.051\,92\,\text{kg}\,\text{mol}^{-1}$	$0.003\,302\,\text{kg}^2/\text{mol}^2$	$3.177\,\text{kg}\,\text{mol}^{-1}$	$-2.131\,\text{kg}^2/\text{mol}^2$

Table A.7.: Faraday efficiency parameters of (3.40) [49]

f_1	f_2
$250\,\text{mA}^2/\text{cm}^4$	0.96

A.2. Thermal Model

Table A.8.: Parameters of the thermal capacity approximation function (3.49)

d_0	d_1
23.947 s/K	4.3325×10^5 J/K

Table A.9.: Densities of H_2, O_2 and H_2O at 293 K according to [36]

ρ_{H_2}	ρ_{O_2}	ρ_{H_2O}
0.089 88 kg/Nm^3	1.429 kg/Nm^3	1000 kg/m^3

Table A.10.: Parameters of the PI controller (3.56)

V_I	V_P
-200	$-1.856e005$

A.3. Rural Grid

Table A.11.: Types of lines in the rural grid

	Linetype A	Linetype B
R in Ω/km	0.125	0.2
X in Ω/km	0.12	0.129
C in µF/km	0.227	0.191
I_R in A	420	285

Table A.12.: Load values of the rural grid

	Load 01	Load 02	Load 03	Load 04	Load 05	Load 06
S in MVA	0.1	1.2	0.2	0.28	0.2	1.2
$\cos(\varphi)$	0.9	0.9	0.9	0.9	0.9	0.9

	Load 07	Load 08	Load 09	Load 10	Load 11	Load 12
S in MVA	0.15	0.07	0.15	0.2	0.1	0.13
$\cos(\varphi)$	0.9	0.9	0.9	0.9	0.9	0.9

	Load 13	Load 14	Load 15	Load 16	Load 17	Load 18
S in MVA	0.2	0.2	0.1	0.12	0.17	0.15
$\cos(\varphi)$	0.9	0.9	0.9	0.9	0.9	0.9

	Load 19	Load 20	Load 21	Load 22	Load 23	Load 24
S in MVA	0.2	0.1	0.05	0.1	0.2	0.1
$\cos(\varphi)$	0.9	0.9	0.9	0.9	0.9	0.9

	Load 25	Load 26	Load 27	Load 28	Load 29	Load 30
S in MVA	0.15	0.3	0.07	0.15	0.3	0.05
$\cos(\varphi)$	0.9	0.9	0.9	0.9	0.9	0.9

	Load 31	Load 32	Load 33	Load 34	Load 35	Load 36
S in MVA	0.05	0.15	0.07	0.05	0.15	0.1
$\cos(\varphi)$	0.9	0.9	0.9	0.9	0.9	0.9

	Load 37	Load 38	Load 39	Load 40	Load 41	Load 42
S in MVA	0.1	0.05	0.3	0.07	0.05	0.05
$\cos(\varphi)$	0.9	0.9	0.9	0.9	0.9	0.9

	Load 43	Load 44	Load 45	Load 46		
S in MVA	0.1	0.1	0.05	0.05		
$\cos(\varphi)$	0.9	0.9	0.9	0.9		

Table A.13.: Assignment of types to the lines in the rural grid

	Line 01	Line 02	Line 03	Line 04	Line 05	Line 06
Type	A	A	A	B	B	A
l in km	0.2	0.5	0.5	0.3	1.2	0.5

	Line 07	Line 08	Line 09	Line 10	Line 11	Line 12
Type	A	B	A	B	B	B
l in km	0.5	1.2	2	0.5	0.5	0.5

	Line 13	Line 14	Line 15	Line 16	Line 17	Line 18
Type	A	B	B	A	A	B
l in km	0.8	0.5	0.7	1.2	0.5	1

	Line 19	Line 20	Line 21	Line 22	Line 23	Line 24
Type	A	B	A	B	A	A
l in km	1.2	1.5	0.5	1.5	1.6	0.7

	Line 25	Line 26	Line 27	Line 28	Line 29	Line 30
Type	A	A	A	A	B	B
l in km	0.7	0.3	1.5	1	1	2

	Line 31	Line 32	Line 33	Line 34	Line 35	Line 36
Type	B	A	B	A	A	B
l in km	0.5	0.5	1	0.8	0.5	0.7

	Line 37	Line 38	Line 39	Line 40	Line 41	Line 42
Type	B	B	B	A	B	B
$\cos(\varphi)$	2	0.3	0.3	3.5	0.5	0.5

	Line 43	Line 44	Line 45	Line 46	Line 47	Line 48
Type	B	B	B	B	B	B
l in km	0.5	0.7	1.5	0.7	0.7	2

A.4. Suburban Grid

Table A.14.: Types of lines in the suburban grid

	Linetype A	Linetype B	Linetype C
R in Ω/km	0.125	0.125	0.206
X in Ω/km	0.111	0.091	0.094
C in µF/km	0.324	0.488	0.430
I_R in A	413	325	255

Table A.15.: Load values of the suburban grid

	Load 01	Load 02	Load 03	Load 04	Load 05	Load 06
S in MVA	0.25	0.25	0.4	0.3	0.15	0.3
$\cos(\varphi)$	0.9	0.9	0.9	0.9	0.9	0.9
	Load 07	Load 08	Load 09	Load 10	Load 11	Load 12
S in MVA	0.2	0.2	0.1	0.2	0.2	0.1
$\cos(\varphi)$	0.9	0.9	0.9	0.9	0.9	0.9
	Load 13	Load 14	Load 15	Load 16		
S in MVA	0.15	0.15	0.15	0.1		
$\cos(\varphi)$	0.9	0.9	0.9	0.9		

Table A.16.: Assignment of types to the lines in the suburban grid

	Line 01	Line 02	Line 03	Line 04	Line 05	Line 06
Type	A	B	B	B	B	B
l in km	0.5	0.2	0.2	0.5	0.3	0.2
	Line 07	Line 08	Line 09	Line 10	Line 11	Line 12
Type	B	C	C	C	C	C
l in km	0.2	0.5	0.5	0.4	0.4	0.4
	Line 13	Line 14	Line 15	Line 16		
Type	C	C	C	C		
l in km	0.4	0.4	0.4	0.4	0.2	

A.5. Standby Battery

Table A.17.: Parameter values of the standby approximation (5.35)

	e_0	e_1
scenario 1	$-7.485\,\text{MWh/day}$	$2.0468\,\text{h/day}$
scenario 2	$-7.485\,\text{MWh/day}$	$2.0468\,\text{h/day}$
scenario 3	$-0.333\,58\,\text{MWh/day}$	$3.1401\,\text{h/day}$

Bibliography

[1] *The National Transmission Grid Study - Transmission System Operation and Interconnection.* U.S. Department of Energy, 2002.

[2] (2013, 09) Germany's power-to-gas pilot projects (2013). [Online]. Available: http://www.powertogas.info/power-to-gas/pilotprojekte.html

[3] APCS. (2013, 09) Synthetic load profiles - consumption forecasts based on load profiles. [Online]. Available: http://www.apcs.at/en/clearing/physical-clearing/synthetic-load-profiles

[4] H. Barthels, W. A. Brocke, K. Bonhoff, H. G. Groehn, G. Heuts, M. Lennartz, H. Mai, J. Mergel, L. Schmid, and P. Ritzenhoff, "PHOEBUS-JÜLICH: An autonomous energy supply system comprising photovoltaics, electrolytic hydrogen, fuel cell," *International Journal for Hydrogen Energy*, vol. 23, pp. 295–301, 1997.

[5] H. Bauer, "Vorteile und Herausforderungen der Kopplung von Gas- und Stromnetzen." Gascade Gasnetz GmbH, 2012.

[6] S. Begluk, M. Boxleitner, R. Schlager, M. Heimberger, C. Maier, and W. Gawlik, *SYMBIOSE und Speicherfähigkeit von dezentralen Hybridsystemen.* 8. Internationale Energiewirtschaftstagung an der TU Wien, 2013.

[7] A. Bergen, L. Pitt, A. Rowe, P. Wild, and N. Djiali, "Transient electrolyser response in a renewable-regenerative energy system," *International Journal for Hydrogen Energy*, vol. 34, pp. 64–70, 2009.

[8] *Gaswirtschaftsgesetz 2011*, BGBl. I Nr. 107/2011 Std.

[9] A. Brinner, "Deutsch-Saudi Arabisches Gemeinschaftsprojekt HYSOLAR (HYdrogen from SOLAR Energy) 1986 - 1995, Was haben wir aus der alkalischen Elektrolyseentwicklung gelernt?" in *NOW-Workshop - Regenerativer Wasserstoff aus der der Elektrolyse*, 2008.

[10] P. Diéguez, A. Ursúa, P. Sanchis, C. Sopena, E. Guelbenzu, and L. Gandía, "Thermal performance of a commercial alkaline water electrolyzer: Experimental study and mathematical modeling," *International Journal of Hydrogen Energy*, vol. 33, no. 24, pp. 7338 – 7354, 2008. [Online]. Available: http://www.sciencedirect.com/science/article/pii/S0360319908012093

[11] T. Douglas, A. Cruden, and D. Infield, "Development of an ambient temperature alkaline electrolyser for dynamic operation with renewable energy sources," *International Journal for Hydrogen Energy*, vol. 38, pp. 723–739, 2013.

[12] E-Control, *Ökostrombericht 2012*, 2012.

[13] ——. (2013, 08) Ausgleichsenergie (AE): Mengen und Aufwendungen von 2003 bis 2010. [Online]. Available: http://www.e-control.at/de/statistik/oeko-energie/ausgleichsenergie-aufwendungen

[14] ——. (2013, 09) Austria's natural gas storages. [Online]. Available: http://www.e-control.at/de/marktteilnehmer/gas/gasmarkt/speicher

[15] ——. (2013, 08) Pressemitteilung, E-Control: Mehr Gasspeichervolumen in Österreich als je zuvor. [Online]. Available: http://www.e-control.at/portal/page/portal/medienbibliothek/presse/dokumente/pdfs/PA-31-03-Speicherkapazitaeten.pdf

[16] C. Edler, *Das österreichische Gasnetz*.   TU Vienna, ESEA, 2013.

[17] E.ON, "Demonstrationsvorhaben Power-to-Gas, Falkenhagen, Conversation with the manufacturer at the Hannover Messe 2013," E.ON edis AG, E.ON New Build & Technology GmbH, Tech. Rep., 2013.

[18] Fachverband der Gas - und Wärmeversorgungsunternehmungen, *Erdgas in Österreich, Zahlenspiegel 2012*, 2012.

[19] R. Gazey, S. K. Salman, and D. Aklil-DHalluin, "A field application experience of integrating hydrogen technology with wind power in a remote island location," *Journal of Power Sources*, vol. 157, pp. 841–847, 2006.

[20] K. Girod and C. Unger, *Abschlussbericht für das BMBF-Verbundprojekt Biogaseinspeisung*.   Fraunhofer-Institut für Umwelt-, Sicherheits- und Energietechnik, 2009, no. 3.

[21] M. Götz, R. Reimert, D. Buchholz, and S. Bajohr, "Storage of volatile renewable energy in the gas grid applying 3-phase methanation," *Internation Gas Union Research Conference*, 2011.

[22] C. Groiss, C. Maier, and J. Scalet, "DSM -Potenziale in einer österreichischen Modellsiedlung," TU Wien Institut für Energiesystem und Elektrische Antriebe, Vorarlberger Energienetze GmbH, Tech. Rep., 2012.

[23] F. Hofmann, A. Plaettner, and F. Scholwin, *Möglichkeiten der Einspeisung von Biogas in das österreichische Gasnetz*, 2005.

[24] Hydrogenics, "HYSTAT-Wasserstofferzeuger," Conversation with CEO Dr. Bernd Pitschak at the Hannover Messe 2013.

[25] F. Incropera and D. De Witt, *Fundamentals of heat and mass transfer*, 5th ed. John Wiley & Sons, 2002.

[26] J. O. Jensen, S. H. Jensen, and N. Tophøj, *Pre-Investigation of Water Electrolysis*. Technical University of Denmark, Risø National Laboratory and DONG Energy, 2006.

[27] O. Kalab, "Standardisierte Lastprofile," Wirtschaftkammer Oberösterreich, Tech. Rep., 2006.

[28] J. Kopyscinski, "Production of synthetic natural gas in a fluidized bed reactor: Understanding the hydrodynamic, mass transfer, and kinetic effects," Ph.D. dissertation, Eidgenössische Technische Hochschule ETH Zürich, 2010.

[29] A. Kugi, *Automatisierung - Vorlesung und Übung*. ACIN TU Wien, 2011.

[30] ——, *Optimierung - Vorlesung und Übung*. ACIN TU Wien, 2013.

[31] W. Leonhard, U. Buenger, C. F., C. Gatzen, W. Glaunsinger, and S. Huebner, *Energiespeicher in Stromversorgungssystemen mit hohem Anteil erneuerbarer Energieträger. Bedeutung, Stand der Technik, Handlungsbedarf*. VDE, 2008.

[32] R. LeRoy, C. Bowen, and D. LeRoy, "The thermodynamics of aqueous water electrolysis," *Electrochem Soc*, vol. 127, pp. 1954–1962, 1980.

[33] M. Lödl, G. Kerber, R. Witzmann, C. Hoffmann, and M. Metzger, "Abschätzung des Photovoltaik-Potentials auf Dachflächen in Deutschland," *11. Symposium Energieinnovation*, 2010.

[34] A. Löewe, *Chemische Reaktionstechnik mit MATLAB und SIMULINK*. WILEY-VCH, 2001.

[35] D. Meissner, "PHOEBUS, die autarke solare Stromversorgungsanlage der Zentralbibliothek des Forschungszentrums Jülich," *Schule und Energie, 1. Seminar Energiesparen, Solarenergie, Windenergie, Jülich, 3. und 4. Juni 1998*, pp. 77–86, 1998.

[36] National Institute of Standards and Technology. (2013, 07) NIST Chemistry WebBook. http://webbook.nist.gov/chemistry/. [Online]. Available: http://webbook.nist.gov/chemistry/

[37] NEL Hydrogen AS, "NEL P-60, Pressurised Electrolyser - Extreme Flexibility; Technical Specifications."

[38] O. Oberzaucher, "Design und Analyse: Systemgekoppeltes Verteilnetz der Zukunft," Master's thesis, Technischen Universität Wien, Fakultät für Elektrotechnik und Informationstechnik, 2013.

[39] D. Oertel, *Energiespeicher - Stand und Perspektiven.* Büro für Technikfolgeabschätzung beim Deutschen Bundestag, 2008.

[40] *Natural Gas in Austria - Gas quality, ÖVGW-Richtlinie G31*, Österreichische Vereinigung für das Gas- und Wasserfach Std., 05 2001.

[41] V. M. Schmidt, *Elektrochemische Verfahrenstechnik: Grundlagen, Reaktionstechnik, Prozessoptimierung.* Wiley-VCH, 2003.

[42] Siemens, "Sitras TCR - Gesteuerter Gleichrichter für die DC-Bahnstromversorgung," Tech. Rep., 2012.

[43] ——. (2013, 08) Pressemitteilung: Siemens baut schlüsselfertiges Gas- und Dampfturbinenkraftwerk in Düsseldorf. [Online]. Available: http://www.siemens.com/press/de/pressemitteilungen/?press=/de/pressemitteilungen/2012/energy/fossil-power-generation/efp201207057.htm

[44] T. Smolinka, M. Günther, and J. Garche, *Stand und Entwicklungspotenzial der Wasserelektrolyse zur Herstellung von Wasserstoff aus regenerativen Energien.* Fraunhofer ISE, FCBAT, 2011.

[45] Statistik Austria, "Durchschnittlicher Stromverbrauch der Haushalte nach Verbrauchskategorien," Tech. Rep., 2008.

[46] M. Sterner, *Bioenergy and renewable power methane in integrated 100% renewable energy systems. Limiting global warming by transforming energy systems*, ser. Erneuerbare Energien und Energieeffizienz / Renewable Energies and Energy Efficiency, J. Schmid, Ed. Kassel University Press, 2009, vol. 14. [Online]. Available: http://www.uni-kassel.de/upress/publi/abstract.php?978-3-89958-798-2

[47] The Wind Power - Datenbank für Windkraftanlagen und Windparks. (2013, 09) Haindorf-Inning Windpark (Österreich). [Online]. Available: http://www.thewindpower.net/windfarm_de_158_haindorf-inning.php

[48] TU Wien/ESEA, *Super-4-Micro-Grid - Nachhaltige Energieversorgung im Klimawandel, Publizierbarer Endbericht.* Österreichische Forschungsförderungsgesellschaft, 2011.

[49] Ø. Ulleberg, "Modeling of advanced alkaline electrolyzers: a system simulation approach," *International Journal of Hydrogen Energy*, vol. 28, no. 1, pp. 21 – 33, 2003. [Online]. Available: http://www.sciencedirect.com/science/article/pii/S0360319902000332

[50] Ø. Ulleberg, T. Nakken, and A. Ete, "The wind/hydrogen demonstration system at Utsira in Norway: Evaluation of system performance using operational data and updated hydrogen energy system modeling tools," *International Journal for Hydrogen Energy*, vol. 35, pp. 1841–1852, 2010.

[51] A. Ursúa and P. Sanchis, "Static-dynamic modelling of the electrical behaviour of a commercial advanced alkaline water electrolyser," *International Journal of Hydrogen Energy*, vol. 37, no. 24, pp. 18 598 – 18 614, 2012. [Online]. Available: http://www.sciencedirect.com/science/article/pii/S036031991202191X

[52] B. Vogl, W. Jank, R. Wurm, M. Stangl, S. Schantl, G. Greutter, and V. Koller-Kreimel, *Erneuerbare Energie 2020 - Potenziale und Verwendung in Österreich*, G. Liebel and M. Schuster, Eds.   Bundesministerium für Land- und Forstwirtschaft, Umwelt und Wasserwirtschaft, 2009.

[53] Windpark Inning-Haindorf, "Generated WP from 11/2011 to 12/2012," Verein Energiewerkstatt. [Online]. Available: http://www.energiewerkstatt.org/